Raytheon

CLOUD MASK

VISIBLE/INFRARED IMAGER/RADIOMETER SUITE ALGORITHM THEORETICAL BASIS DOCUMENT

Version 3: May 2000

North Larsen

Allen Huang, Science Team Member

University of Wisconsin, Madison

RAYTHEON SYSTEMS COMPANY
Information Technology and Scientific Services
4400 Forbes Boulevard
Lanham, MD 20706

SBRS Document #: Y2412

NPOESS COMPETITION SENSITIVE

EDR: CLOUD MASK

Doc No: Y2412

Version: 3

Revision: 0

	Function	Name	Signature	Date
Prepared by	EDR Developer	NORTH LARSEN		4/15/00
Approved by	Relevant IPT Lead	GLENN J. HIGGINS		5/3/00
Approved by	Chief Scientist	P. ARDANUY		5/3/00
Released by	Program Manager	H. BLOOM		5/5/00

TABLE OF CONTENTS

Page

LIST OF FIGURES

LIST OF TABLES

Page

GLOSSARY OF ACRONYMS

ARM	Atmospheric Radiation Measurements
ADEOS2	Advanced Earth Observing Satellite-2
AERI	Atmospheric Emitted Radiance Inferometer
AERONET	Aerosol Robotic NETwork
AMSR	Advanced Microwave Scanning Radiometer
ARMCAS	Arctic Radiation Measurement in Column: Atmosphere-Surface
ATBD	Algorithm Theoretical Basis Document
ATSR	Along-Track Scanning Radiometer
AVHRR	Advanced Very High Resolution Radiometer
AVIRIS	Airborne Visible Infrared Imaging Spectrometer
BBSS	Balloon-Borne Sounding System
BLC	Belfort Laser Ceilometer
BRDF	Bidirectional Reflectance Distribution Function
BRF	Bidirectional Reflectance Factor
BT	Brightness Temperature
CAR	Cloud Absorption Radiometer
CLAVR	Clouds from AVHRR
CLS	Cloud Lidar System
CMIS	Conical Scanning Microwave Imager/Sounder
CRIS	Cross-track Infrared Sounder
CSPOT	Cimel Sunphotometer
CVP	Cloud Validation Plan
DEM	Digital Elevation Module
DOC	Department of Commerce
DOD	Department of Defense
EDC	EROS Data Center
EDR	Environmental Data Requirement
EOS	Earth Observing System
FIRE-ACE	First ISCPP Regional Experiment – Arctic Cloud Experiment
FOV	Field of View
FWHM	Full-width Half-maximum
GLI	Global Imager
GUV	Ground based Ultraviolet
HCS	Horizontal Cell Size

HITRAN	High Resolution Transmission Model
IABP	International Arctic Buoy Program
IPO	Integrated Project Office
IPT	Integrated Planning Team
IRT	Infrared Thermometer
ISCCP	International Satellite Cloud Climatology Project
LANDSAT	Land Satellite
LLLS	Low Level Light Sensor
LUT	Look-Up Table
MAS	MODIS Airborne Simulator
MCM	MODIS Cloud Mask
MFRSR	Multi-Filter Rotating Shadowband Radiometer
MISR	Multiangle Imaging Spectroradiometer
MLP	Micropulse Lidar
MODIS	Moderate Resolution Imaging Spectroradiometer
MODTRAN	Moderate Resolution Atmospheric Radiance and Transmission Model
MWR	Microwave Water Radiometer
NASA	National Aeronautics and Space Administration
NDII	Normalized Differential Ice Index
NIP	Normal Incidence Pyrheliometer
NOAA	National Oceanic and Atmosphere Administration
NPOESS	National Polar-orbiting Operational Environmental Satellite System
NPP	Net Primary Production
NVCM	NPOESS VIIRS Cloud Mask
OMPS	Ozone Mapping Profiling Suite
PAN	Panchromatic
PSC	Polar Stratospheric Clouds
PSP	Precision Spectral Pyranometer
RDQI	Radiometric Data Quality Indicator
RGB	Red-Green-Blue
RL	CART Raman Lidar
RMS	Root Mean Square
RSS	Rotating Shadowband Spectrometer
SCARB	Smoke, Clouds, and Radiation – Brazil
SDR	Sensor Data Requirement
SERCAA	Support of Environmental Requirements for Cloud Analysis and Archive

SMET	Surface Meteorology
SMOS	Surface Meteorological Observation System
SNR	Signal-to-Noise Ratio
SRD	Sensor Requirements Document
SRR	Systems Requirements Review
SUCCESS	Subsonic Aircraft Contrail and Cloud Effects Special Study
TARFOX	Tropospheric Aerosol Radiative Forcing
TASC	The Aerospace Corp.
TBD	To Be Determined
TBR	To Be Resolved
TOA	Top-of-Atmosphere
UAF	University of Alaska, Fairbanks
UV	Ultraviolet
UW	University of Wisconsin
VCM	VIIRS Cloud Mask
VIIRS	Visible/Infrared Imager/Radiometer Suite
VTLC	Video Time-Lapsed Camera
WINCE	Winter Cloud Experiment
WSI	Whole-Sky Imager

ABSTRACT

The VIIRS Cloud Detection Algorithm determines if a given view of the Earth's surface is cloud-contaminated or cloud free. This detection results in the generation of a pixel-level cloudy/not cloudy mask at the HSR of the VIIRS sensor. This mask is an intermediate or ancillary data product for the retrieval of cloud and other EDRs (e.g., sea surface temperatures). To perform cloud detection the VIIRS radiance data for radiometric channels 0.556, 0.67, 0.859, 1.375, 1.61, 3.7, 4.05, 8.6, 10.8, and 12.0 microns are used, the imagery resolution channels 0.645, 0.859, 1.61, 3.7, and 11.45 microns are used, and additional ancillary data.

The ancillary data required as input to the cloud detection algorithm include: a global land/sea map, ecosystem map, sun/sensor geometry, and the most recent snow/ice map. Additional ancillary data that may potentially be used are from the following sensors: Cross-track Infrared Sounder (CRIS), Conical Scanning Microwave Imager/sounder (CMIS), and the Visible/Infrared Imager/Radiometer Suite (VIIRS) Day Night Band (DNB). The full value of these additional ancillary data sources requires additional research. Other tests will be explored, time permitting, to aid in cloud/no cloud classification. These include temporal consistency and spatial variability tests, applied to radiance and brightness temperature values within pixel regions.

Using the VIIRS radiance data in combination with the ancillary data the cloud detection is performed at both the imagery and radiometric pixel resolution. The cloud detection involves a series of thresholding and ratioing tests using the solar reflectance, and thresholding and differencing tests using the thermal Brightness Temperature (BT). The threshold values for the various tests are dependent upon the dominant regional classification, or surface type, of the pixel to be tested. The tests applied to generate the cloud masks have a heritage from the Advanced Very High Resolution Radiometer (AVHRR) (Clouds from AVHRR [CLAVR], Stowe *et al*., 1988), and the Moderate Resolution Imaging Spectroradiometer (MODIS) (Ackerman *et al*., 1997). Additional cloud detection thresholding and ratioing techniques are presently under development.

1.0 INTRODUCTION

1.1 PURPOSE

This Algorithm Theoretical Basis Document (ATBD) explains the mathematical background to derive the Environmental Data Requirement (EDR) of the VIIRS Cloud Mask (VCM). This EDR is a binary cloudy/not cloudy result, which is part of the Cloud Cover/Layers EDR. In addition, this document provides an overview of the required input data, the physical theory of the radiative transfer, assumptions and limitations, and a sensitivity study of the described algorithm. The one EDR described in this document is part of the National Polar-orbiting Environmental Satellite System (NPOESS)/VIIRS team software package of a total of 29 Environmental Data Requirements (EDRs). Parameters relevant for the EDR VCM are displayed below.

Table 1. Parameters in the VCM Product.

Name	Units	Definition/Comments
Spectral radiance (L)	W/(m^2 sr μm)	Radiant energy per time-area-solid angle wavelength interval
Brightness Temperature	K	Brightness temperature for a given channel of the sensor, derived from spectral radiance.
Equivalent reflectance (ρ_{equiv})	None	$\pi \times$L divided by normal incidence TOA irradiance
Normal incident TOA Irradiance	W/(m^2 μm)	Normalized incident TOA Irradiance in specific channel
Terrain-referenced geometric parameters	Deg	Solar- and observer geometry
Retrieval quality indicators	vary	Determine the quality assessment of the VCM

1.2 SCOPE

This document covers the theoretical basis for the generation of the VIIRS EDR VCM Algorithm. Future developments in the theoretical approach, as well as the satellite design, may result in modifications of the algorithms presented here.

The purpose and scope of this document are described in this section. Section 2 gives an overview of the cloud mask generation objectives. Section 3 describes the VCM, its input data, the theoretical background, and some practical considerations. Section 4 lists the assumptions and limitations valid for the VCM.

1.3 VIIRS DOCUMENTS

This document contains references to other VIIRS documents. These are given in italicized brackets, e.g., *[V-29]* CLOUD MASK. The VIIRS documents cited in this document are listed below:

[V-0] VIIRS Experiment Overview

[V-4] Aerosol Optical Thickness

[V-5] Aerosol Particle Size Parameter

[V-8] Cloud Cover/Layers

[V-14] Albedo (Surface)

[V-16] Normalized Difference Vegetation Index

[V-18] Vegetation Index/Surface Type

[V-24] Ocean Color/Chlorophyll

[V-27] Atmospheric Correction Over Ocean

[V-28] Atmospheric Correction Over Land

1.4 REVISIONS

This is the third version of this document, dated May 2000. The original version of this document was dated September 3, 1998.

2.0 EXPERIMENT OVERVIEW

2.1 INSTRUMENT CHARACTERISTICS

The VIIRS sensor will provide global coverage every day.

Table 2. VIIRS Channels. The VIIRS Channels Indicated Will be Used for the VCM

Band	Wave (µm)	BW (µm)	VCM Bands
DNB	0.7000	0.4000	VCM
Ch2w2	0.4120	0.0200	
2	0.4450	0.0180	
Ch8	0.4880	0.0200	
4	0.5550	0.0200	
5i	0.6450	0.0500	VCM
OC2	0.6720	0.0200	VCM
OC3	0.7510	0.0150	
6i	0.8650	0.0390	VCM
6r	0.8650	0.0390	VCM
Cd1	1.2400	0.0200	
7	1.3780	0.0150	VCM
8i	1.6100	0.0600	VCM
8r	1.6100	0.0600	VCM
9	2.2500	0.0500	
10iw	3.7400	0.3800	VCM
10r	3.7000	0.1800	VCM
SST2	4.0500	0.1550	VCM
SST4	8.5500	0.3000	VCM
11	10.7625	1.0000	VCM
12iw	11.4500	1.9000	VCM
12r	12.0125	0.9500	VCM

Additional details on the instrument design are provided in the VIIRS Experiment Overview *[V-0]*. Note that VIIRS bands have been given new names, as described in the system specification.

2.2 OBJECTIVES OF THE VIIRS CLOUD MASK

The objective of the VCM is to determine if a given Field of View (FOV) has a cloud present. The VIIRS VCM is defined as the pixel level flag which indicates when a line segment extending between the sensor and a given area of the Earth's surface is intersected by a cloud. The cloud mask EDR is a binary cloudy/not cloudy flag operating at the pixel level using VIIRS radiance data. Aggregation of the cloud mask to a larger HCS is performed to retrieve the Cloud Cover/Layers EDR. The VCM operates at a radiometric pixel resolution (742 m), and at the imagery pixel resolution (371 m). It is noted to the reader that not only is the VCM an EDR, but it is crucial as a first step in evaluating any scene before further processing is begun to retrieve the many other VIIRS EDRs. Also output by the VCM in addition to the binary cloudy/not cloudy EDR are many processing flags and test result indicators, which are used by other EDRs in the VIIRS processing architecture.

2.3 HISTORICAL PERSPECTIVE

Cloud masking, or screening, involves the discrimination between clear and cloudy pixels within an image. Excellent reviews of the many cloud detection methods can be found in the literature (Ackerman *et al*., 1997; Hutchinson and Hardy, 1995; Kriebel and Saunders, 1988; Stowe *et al*., 1995; Goodman and Henderson-Sellers, 1988; and Rossow, 1989). The methods used in detecting clouds are generally based upon radiance and Brightness Temperature (BT) thresholding and statistical techniques which make use of the spectral and textural features in the imagery. The radiance and BT thresholding techniques performed by the VCM work on a pixel-by-pixel basis. Single or multi-channel thresholds are used to divide clear from cloudy pixels. Thresholding tests performed by the VCM have a heritage from CLAVR and MODIS. Statistical techniques use groups of adjacent pixels to recognize cloud apparent behavior.

2.4 CLOUD MASKING APPROACH

The VCM is essentially derived from the MODIS Cloud Mask (MCM) multi-channel cloud masking techniques (Ackerman *et al*., 1997), which in turn have their heritage in other algorithms. These include the Support of Environmental Requirements for Cloud Analysis and Archive (SERCAA) algorithm (Gustafson *et al*., 1994), and Clouds from AVHRR-Phase I (CLAVR-1) algorithm (Stowe *et al*., 1998). In using heritage technology the VCM has used the latest developments from cutting edge research. This research has been conducted by the MODIS cloud research team at the University of Wisconsin, headed up by Dr. Steve Ackerman, and the CLAVR-2 algorithm as it developed by scientists at NOAA, lead by Dr. Larry Stowe of the NPOESS Integrated Project Office (IPO). A third cloud mask used to improve the VCM is presently being developed for cloud detection in the cryosphere. This is cloud mask is being developed for the Global Imager (GLI) instrument on the ADEOS2 satellite (Stamnes *et al*., 1998), by Dr. Knut Stamnes' Radiative Transfer group at the University of Alaska Fairbanks (UAF). When new cloud detection techniques are developed and proven to be effective, the modularized coding of the VCM will allow for these techniques to be added.

3.0 ALGORITHM DESCRIPTION

3.1 PROCESSING OUTLINE

The VCM is developed from a hybrid of the MODIS/CLAVR cloud masks (Ackerman *et al*., 1997; Stowe *et al*., 1998). As a hybrid algorithm, it combines the best cloud detection features from both of these cloud detection algorithms. The overall processing structure of the VCM is directly related to the MODIS Cloud Mask algorithm processing structure, developed by Dr. Steve Ackerman's research team at the University of Wisconsin. The author would like to extend his gratitude to the individuals on Dr. Ackerman's team in their development of the MCM algorithm that was used as a framework for the VCM.

Generation of the VCM occurs routinely as part of the first level of EDR processing, residing in the SDR module. The VCM pixel level results are then used at a pixel level by the other EDRs. The VCM results also undergo a conversion from a pixel level cloud mask to a Horizontal Cell Size (HCS) in the VIIRS Cloud Cover EDR. VCM output are used by the many other EDRs which are dependent on cloud masking. The VCM does cloud tests at both the radiometric resolution, using the radiometric bands, and at the higher Imagery resolution, using the Imagery bands. The pixel level detection is performed using a limited number of cloud thresholding tests, and spatial homogeneity tests upon the 2x2 imagery bands. The Imagery resolution tests use thresholding at the imagery resolution. Imagery resolution tests used by CLAVR-1 are used in the VCM. These multi-pixel contrast and thresholding tests are done using the five Imagery and one. Use of the the imagery resolution bands for cloud detection allows for the sub-pixel level clouds to be more easily detected.

Output from the VCM is 6 bytes (48 bits) for each radiometric resolution pixel. Table 3 summarizes the VCM Intermediate Product (IP) output for each radiometric resolution pixel.

Table 3. 48 Bit Intermediate Product output of the VCM

BYTE	Flag	Bit #	Note (bit results indicate)
1	Cloud Mask Quality Flag	1	1= Mask Okay/0=Mask Questionable
	Binary Cloud EDR result	2	1= cloudy/0=not cloudy
	Cloud Imagery Resolution Flag	3-6	1=cloudy/0=not cloudy (each bit is a pixel of the 2x2 imagery resolution pixels nested in the radiometric resolution pixel), 1111 = all cloudy, 0000=all not cloudy
	Cloud Confidence Flag	7-8	4 confidence levels of Cloud EDR Flag, 11= Confident Cloudy, 10=Probably Cloudy, 01= Probably Clear, 00=Confident Clear
2	Sun Glint Flag	9-10	11= Geometry Based Sunglint, 10= Wind Speed Based Sunglint, 00= No Glint (1 spare flag 01)
	Snow Surface	11	1=Snow/Ice, 0=No Snow/Ice
	Surface Type	12-14	111=Land, 000=Water, 010=Coastal, 011=Desert Other 5 flags (101,110,100,001,010) reserved for additional surface types used in future
	Non-Cloud Obstruction	15	1=Yes, 0=No
	Thin Cirrus Detected (Daytime)	16	1=Yes, 0=No
3	Cloud Phase	17-18	11=water, 00=ice, 10=mixed, 01= unknown
	Pixel Within 2 of a cloudy pixel	19	1=yes, 0=no (radiometric pixel size considered)
	Shadow Flag	20	1=yes, 0=no
	High Cloud Flag	21	1=yes,0=no
	Low Cloud Flag	22	1=yes,0=no
	Fire Detected	23	1=yes, 0=no
	Day/Night	24	1=Day,0=Night
4	Cloud Test Flags	25-32	4 Cloud Test Results indicators 1=tested/0=not tested and 1=cloud detected/0=no cloud detected. Each Cloud test done has a 2 bit flag which tells if a pixel was tested and if it passed or failed.
5		33-40	4 Cloud Test Results indicators (see Byte 4)
6		41-44	2 Cloud Test Results indicators (See Byte 4)
		46-48	Spare Bits (2 more cloud tests allowed in future)

A conceptual overview of the VCM algorithm is displayed in Figure 1. The data input to the VCM is illustrated in the ellipsoids above the 'black box' in which the VCM is contained. Output from the VCM is illustrated at the bottom of Figure 1. Note that the output data which contain question marks are To Be Resolved (TBR). The output data are reported at a pixel level. For the multi-pixel tests, the output data are reported at an aggregated pixel resolution.

The VCM box in Figure 1 has been expanded in order to assist in explaining how the VCM algorithm processes the data. Figures 2 through 6 depict the expansion of the VCM and show the general flow of the algorithm at its present state.

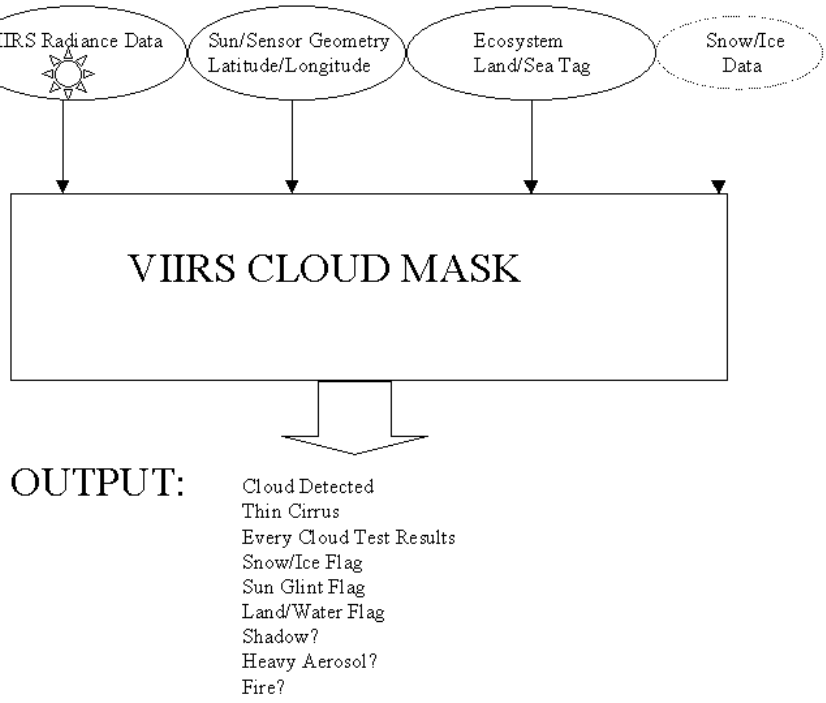

Figure 1. Conceptual overview of the EDR VCM.

The first modules (Figure 2) of the VCM show the processing steps for the cloud mask. These are performed in a loop over a given scan line of the image being masked. First, the arrays for the algorithm are defined. This sets up the appropriately sized arrays for channel radiances, latitude, longitude, channel BTs, channel reflectances, sun/sensor geometry, ecosystem, and others. Once these arrays have been defined, they are then filled with data read in from ancillary data products (Section 3.2), VIIRS radiance data, and sun/sensor data. In order to perform BT thresholding tests, the radiances for the VIIRS thermal channels are assumed to have been converted to BT values before the VCM in the SRD Module. These are placed in the appropriate arrays. Due to limited data flow from the sensor to the algorithms, the additional sun/sensor relative azimuthal and reflectance angles are assumed to be calculated previous to the VCM for the given FOV. The background beneath the pixel being masked is then determined. The land/ocean mask, sun glint mask, and ecosystem are applied. Logical arrays are defined along the entire scan line which define the pixel in terms of its background. This is necessary to define which thresholding tests are to be performed later in the algorithm, as well as to set the

appropriate cloud detection threshold values. The BT and Reflectance values are then unscaled. Note, however, that this unscaling step may not be necessary if no scaling was done to the radiance before the algorithm began processing. Scaling has often been performed in cloud mask program architectures in the past to decrease the overall data flow rate. The solar radiance channels are then converted to reflectances, and the thermal radiance channels are converted to BTs, if either have not been converted previous to the cloud mask. These reflectances are used in the thresholding cloud detection tests, while the BTs are used in differencing tests which are employed to detect the presence of a cloud.

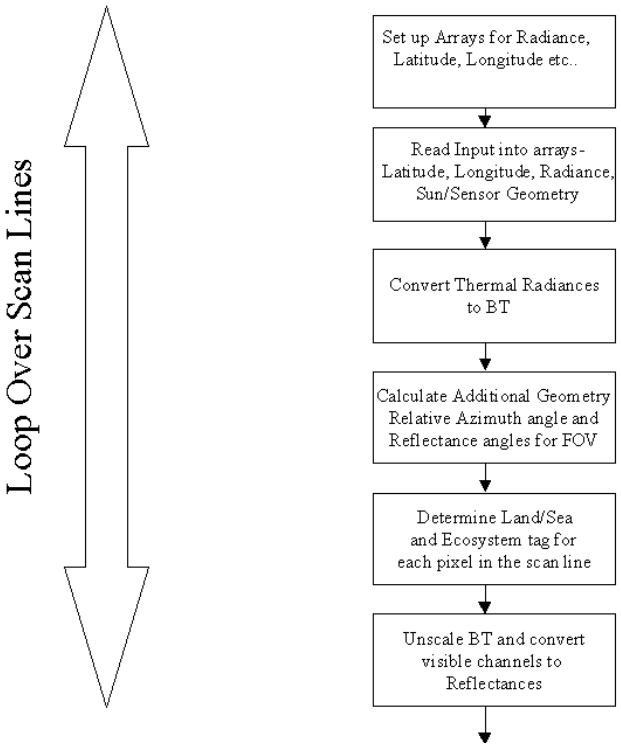

Figure 2. Flowchart of the VCM.

Once a given scan line of an image is prepared, the loop along the scan line is performed. Each scan line is processed within the loop over the scan lines. For an image, a simple way to envision this looping process (Figure 3) is the following. If, along a scan line is the horizontal x, and y is the vertical, there is a loop over x done within a loop along y. To facilitate the cloud tests, a context region is first set up. This is an N by N region, with N defined by the user. At present the context region has N set at the value N=1, this corresponds to the VIIRS radiometric pixel resolution. In the future, if cloud contrast tests are performed upon the bands for mask output at a coarser resolution, the context region considered might be increased in size. An array is then filled with the radiometric band BT, reflectance, and radiance values for the pixels within the N by N region. This N by N region is set up in order to be slid along a given scan line. The central pixel will have pixel level tests performed upon it. And, in future algorithms, the larger region surrounding the center pixel will have the capability to have contrast and statistical tests performed upon it. Contrast and threshold tests will also be performed upon the five 2x2 Imagery and DNB channels which nest within the VIIRS radiometric resolution pixels; tests under consideration are CLAVR in heritage. In the MCM (Ackerman *et al*., 1997), it has proven

necessary to perform an averaging of the thermal channels over the entire context region, in order to minimize the thermal noise. Presently, this is not being done for the BT threshold tests. In the future, this averaging may be performed if it demonstrates an improvement in cloud masking. The cloud mask array results are then cleared prior to cloud masking. The ancillary data logic flags are subsequently set for the pixel region being masked. This means that the region is defined as being within the following categories: land/water, in a possible sun glint geometry, day/night, or in a polar region. This is a crucial step. The definition of the region will control the dataflow of the algorithm, and determine which cloud masking tests are performed and thresholds applied. In sun glint regions there will still be a cloud mask generated. This cloud mask, however, will only employ the thermal cloud detection tests which are unaffected by sun glint. The region is then tested for snow/ice using Normalized Differential Ice Index (NDII) tests developed by D. Hall (Hall *et al*., 1995) and K. Stamnes (Stamnes *et al*., 1998). After the arrays have been set up in the context region the masking occurs.

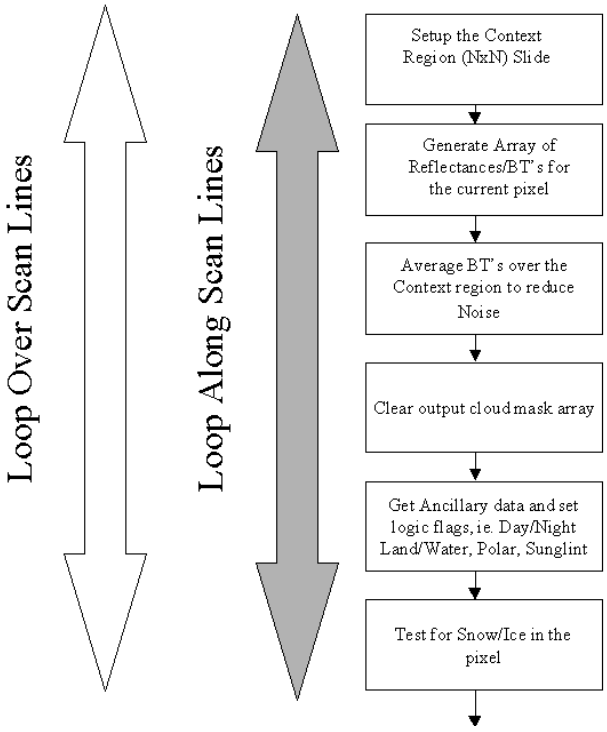

Figure 3. Flowchart of the VCM.

The crucial masking occurs in the first box depicted in Figure 4. This box is expanded in Figure 7 and explained in more detail later in this processing description. Along with the cloud detection (performed on a radiometric pixel level and at the imagery resolution), the specific cloud test which flagged the cloudy pixel will be reported. By reporting the cloud test which was successful, the capabilities of specific cloud tests can be better assessed and the detection thresholds adjusted appropriately. The presence of high versus low level clouds, classification of cloud thermodynamic phase, and automated cloud typing are also performed. Another capability of this cloud mask is the use of a confidence code upon each pixel, this confidence technique is what is presently employed by the MCM (Ackerman *et*

al., 1997). The setting of an absolute threshold to distinguish between completely cloudy and clear is quite abrupt in some cases. A range of values between the definite confident clear and definite confident cloudy is established to identify pixels confidence. From experience with the MCM, the author notes these regions are commonly the cloud edge regions. Assessment of confidence of the cloudy vs. clear will assist other EDR algorithms, which are dependent upon the VCM to judge the quality of the cloud flagged pixels. A similar series of confidence levels are also performed for the cloud phase determination.

The confidence flag methodology applied to establish four levels of cloud confidence is similar to what is used in the MCM (Ackerman *et al*, 1997). The reasoning behind using these confidence levels is because as one approaches the threshold limits, the certainty or confidence in the labeling of a pixel as being cloudy or not cloudy becomes uncertain. As such an individual confidence flag is assigned to each single pixel test, and the value of this confidence is a function of how close the observation is to the thresholds. All of the individual confidence flags are combined to produce the final cloud mask radiometric resolution EDR flag. The four confidence levels are designed to provide information on how much confidence a user of the cloud mask can place upon the result. Each test is given a value between 0 and 1, representing increasing confidence that the pixel has clear sky conditions. Figure 5 is a graphical representation of how a confidence level is assigned for a given spectral test. The abscissa represents the observations and the ordinate the confidence of clear sky conditions. In this figure the observation greater than γ is high confidence clear, while an observation with a value less than α is cloudy. Likewise between α and β is probably cloudy confidence, and β and γ is probably clear confidence. These high confidence clear and cloud thresholds, γ and α respectively, are determined from observations and/or theoretical simulations. The MODIS Cloud Mask team has found the S function may be applied to assign confidence, the VCM has adopted a similar approach. In the final cloud mask only four levels of confidence are provided, these confidences are based upon how close the observed value is to a set of thresholds. These individual confidence levels are combined to determine if a final decision of cloudy or clear is determined, with the probably cloudy and confident cloudy indicating the binary EDR Cloudy result, and the probably clear and confident clear indicating the binary EDR Not Cloudy result. The way in which the bits are arranged in the VCM and also the modularized coding of the VCM will allow the use of a full MODIS Cloud Confidence determination if this is proven by MODIS to be a beneficial methodology. For the Imagery resolution 2x2 nested in each radiometric pixel if only 1 of the 4 pixels indicates a cloud then the results are probably cloudy, if 2 or more indicate cloud presence then the pixel is confident cloudy, and if none indicate cloud presence then it is confident clear.

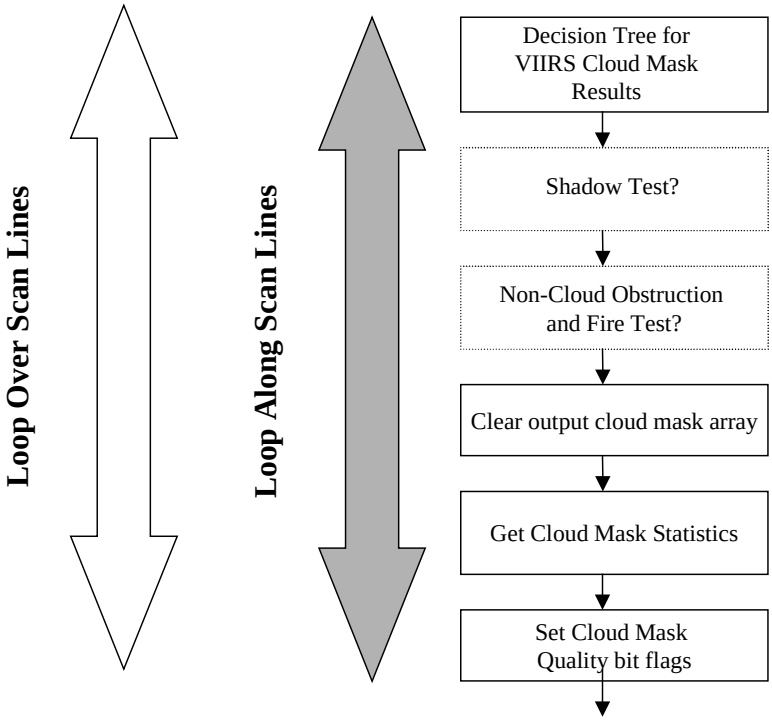

Figure 4. Flowchart of the VCM.

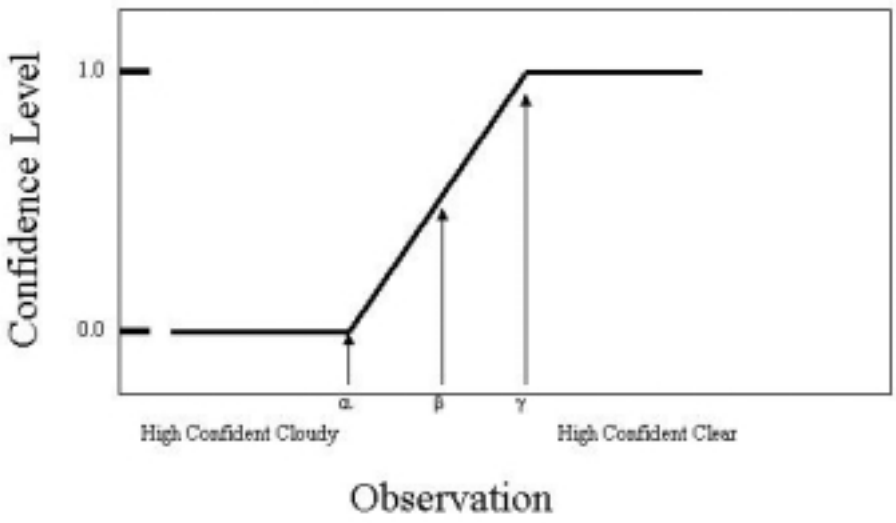

Figure 5. A graphical depiction of the confidence thresholds used in cloud detection

Once a cloud mask result has been returned for the context region or individual pixel, there are several alternative tests which are then performed. A shadow test is then performed (see Section 3.3.4.2). This test determines if there are shadows within the regions where clouds were not detected. Detection of cloud on cloud shadows and cloud shadow on snow/ice are issues for

further research. These detections are not presently being considered. The next test performed over the pixel region is a test for a non-cloud obstruction. This is a non cloud obstruction test (see Section 3.3.4.1). The cloud mask statistics from the context region are then set into the proper arrays. The cloud mask flags are also set, along with quality flags for use by other EDRs in assessing the cloud mask performance. When this has been done, the loop along the scan line is complete. The loop over the scan lines is continued with the next scan line. This loop will be continued until all scan lines of the image have been masked.

The final step in the loop over scan lines is depicted in Figure 6. For each scan line the output of the cloud mask is written out as a stream of 48 bits for each pixel within the region. The output also includes quality flags indicating the performance and confidence of the cloud mask, and the Imagery resolution cloud mask results. This Cloud Mask IP was explained earlier.

Data are then rebuffered for the next scan line, thus freeing up arrays with appropriate indexing. The loop over the scan lines is then resumed until all scan lines in the image have been masked. At this point, the statistics of the cloud mask image as a whole are output. This step is performed for the inspection of the analyst. These image statistics may be used by the cloud cover EDR or imagery EDRs in the future. If not, that step can be removed from the final algorithm structure.

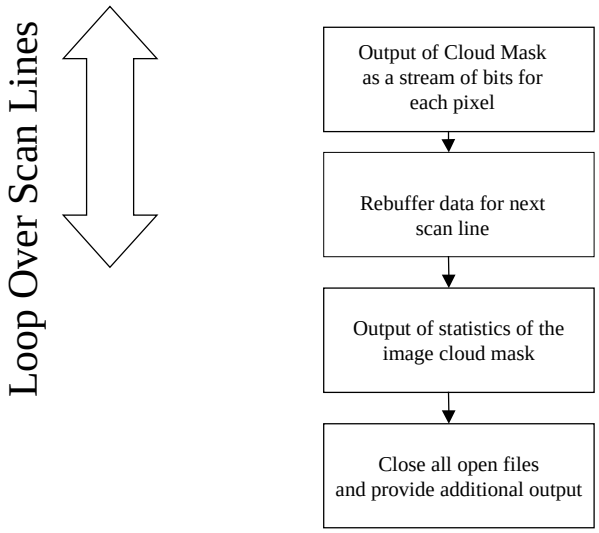

Figure 6. Flowchart of the VCM.

Figure 7 illustrates the flow of the VCM within the first module of Figure 4. For a given pixel, the knowledge of the underlying surface type determines which specific cloud tests are performed. The flow of the algorithm determines the cloud tests and threshold settings for the pixel, based upon the underlying surface type. The underlying surfaces are designated as polar, land, ocean, desert, and coastal. The tests performed for these specific regions will be discussed in Section 3.3.5. As the algorithm develops, additional surface type modules may be added, based on whether more specific threshold differences are found to improve cloud detection.

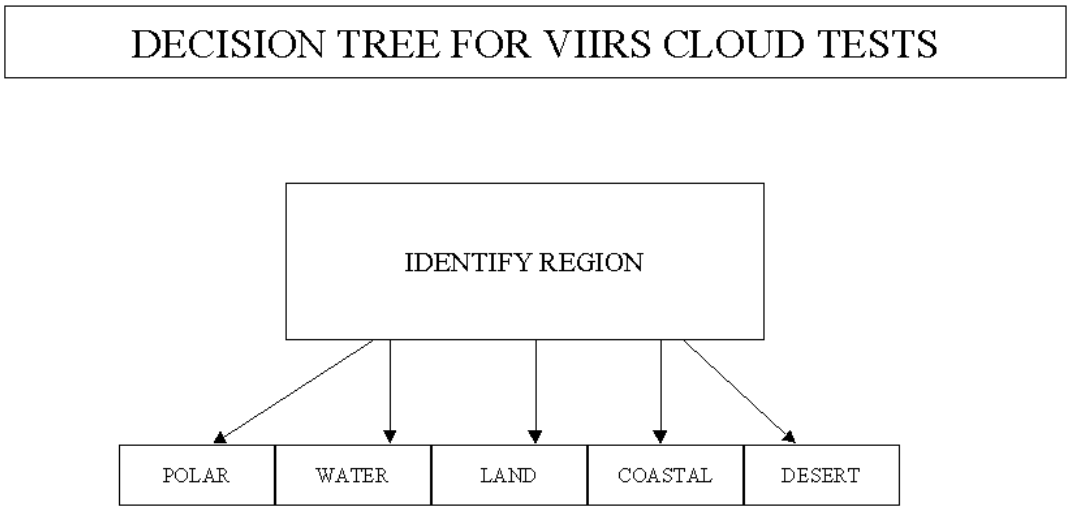

Figure 7. Conceptual overview of the pixel region classification by the SDR VCM.

3.2 ALGORITHM INPUT

3.2.1 VIIRS Data

Table 4 lists the required ancillary data. All of the input ancillary data are explained in greater detail in the following section.

Table 4. Ancillary VIIRS data for the VCM.

Input Data	Source of Data
Land/Water Tag	EROS Data Center
Ecosystem Map	Olson/Loveland
Topographical Map	USGS/EDC
Radiometric Quality Indicator	VIIRS
Most Recent Snow/Ice Map	VIIRS/CMIS/RADARSAT
Sun/Sensor Geometry	VIIRS
Geolocation Data	VIIRS

3.2.1.1 Land/Water Tag

The VCM requires a land/water map to discriminate land from water. Land and water possess different surface reflective properties. These properties affect the thresholds applied in discriminating clear sky from cloud. We will need the best quality land/water map available. Presently the VCM uses the 1 km resolution world map provided from the EROS Data Center (EDC). A possible future solution is to use the data product generated by the MODIS instrument. After launch it is hoped that a VIIRS Land/Water product is available for use.

3.2.1.2 Ecosystem Map

This data is required to discriminate different land types. Various land types possess different reflective properties. The reflective properties need to be known to properly develop and identify the correct thresholds to be applied in cloud tests. The Olson map of ecosystems (10 minute resolution) is being used for global processing, while over North America, Tom Loveland's ecosystem map (1 km resolution) is being applied. The MODIS Land Cover Classification is planned to be used in future development stages for this algorithm. Once NPOESS is operating, and global data are being acquired and updated regularly, the VIIRS Surface Type EDR can be applied. At this level, this will be an IP product.

3.2.1.3 Topographical Map

Presently this is not being used within the VCM. However, in the future, a topographical map, or Digital Elevation Model (DEM) may be applied to assist in defining rugged versus plateau terrain. This is needed to determine the pixel elevation, define terrain type, identify topographically induced shadowing, modify surface reflectances, and to assist in cloud versus snow/ice cover discrimination. The GTOPO30 (USGS/EDC) DEM, with approximately 1 km resolution, is planned to be used in the future. The quality of the topographical data, and the methodology utilized, will be developed with a heritage of MODIS technology.

3.2.1.4 Radiometric Data Quality Indicator

The Radiometric quality of the input radiances are described by the Radiometeric Data Quality Indicator (RDQI). A threshold of RDQI ≥ 1.0 must be obtained to start the VCM retrieval procedure.

3.2.1.5 Snow/Ice Map

Snow/Ice discrimination is required. This snow/ice map is needed to decide which cloud detection tests will be applied, and also to adjust thresholds of several tests. Spectrally, snow/ice and clouds have many similar features. A snow/ice map will decrease the misclassification of snow/ice as clouds. Presently the VCM uses an NDII Snow/Ice threshold detection technique (Hall, 1996). The snow/ice mask is planned to be a combined result of CMIS snow cover EDR, CMIS fresh water ice EDR, CMIS sea ice edge motion EDR, VIIRS snow cover EDR, VIIRS fresh water ice EDR, thresholding techniques developed by MODIS, and global climatological records of sea ice extent and location in the future. What is planned to be used is the most recent snow/ice knowledge within the pixel region being masked, this will be a stored global array which is updated within the VCM by snow/ice tests. Knowledge of snow/ice is also needed beneath the clouds by other Cloud EDRs following the VCM.

3.2.1.6 Sun/Sensor Geometry

The sun viewing geometry (including solar and azimuthal angles), and the sensor viewing geometry are required for the VCM. These are used for setting some reflectance threshold tests. The data will be used to look for sun glint effects; set, apply, or adjust thresholds for cloud detection tests; assist in eliminating optically thick aerosol-laden paths (which can be misidentified as clouds); assist in the identification of cloud shadows; and to determine if a pixel

is in the day or night regime. The night regime is defined as when the solar zenith angle exceeds 85 degrees.

3.2.1.7 Geolocation Data

The latitude and longitude of the surface being viewed is required by the VCM. The surface coordinates allow the land/sea/ecosystem information to be obtained from the land/water and ecosystem maps.

3.2.1.8 Surface Temperature Maps

Surface temperature maps are presently not being used in the VCM. The surface temperature map, when available, may be used as ancillary input data to the VCM. A surface temperature map for both land and sea is needed to enhance cloud detection. Low surface temperatures can be misidentified as clouds in some thermal cloud detection tests with a lack of daytime solar radiance measurements. Also, thermal threshold tests, for cloud detection will need to be modified using surface temperature data. The surface temperature map is expected to come from a combination of the CMIS Sea Surface Temperature EDR, CMIS Land Surface Temperature EDR, CRIS Vertical Temperature Profile EDR, VIIRS Ice Surface Temperature EDR, VIIRS Land Surface Temperature EDR, VIIRS Sea Surface Temperature EDR, ground based *in situ* surface temperature measurements, and sea ice based *in situ* surfaces measurements from the International Arctic Buoy Program (IABP). These surface maps may be used for establishing thresholds over a region for cloud detection tests. The primary benefits achieved from using surface temperature maps would be for nighttime cloud tests.

3.2.1.9 Clear Sky Surface Radiance/Reflectance Composite Maps

Clear sky radiance/reflectance composite maps are presently not being used in the VCM. Clear sky radiance composite maps may be needed to improve cloud detection. Clear sky radiance maps will allow cloud detection thresholds to be set and evaluated, and improve cloud detection. These clear-sky composite maps are expected to be composed of clear sky VIIRS radiance measurements, clear sky OMPS radiance measurements, clear sky CRIS radiance measurements, and clear sky CMIS radiance measurements. Dramatic seasonal differences in vegetated surface reflectances may require monthly or seasonal clear sky radiance composite maps at a regional level. In many cases, just using the most recent clear sky radiance map will assist in cloud detection. These radiance composite maps are not required for the cloud mask, but if they are available they may be used.

3.2.1.10 VIIRS DNB and Imagery Channels

The VIIRS DNB Top of Atmosphere (TOA) is not presently used for VIIRS cloud detection. It is believed that the DNB may be useful for cloud detection at nighttime when lunar illumination is concurrent. The usefulness of the DNB for this application needs to be investigated, along with the thresholds for the cloud detection tests associated with it.

Use of the Imagery Channels BT and reflectances is presently done to improve upon the detection of subpixel clouds within pixels which the imagery channels nest with other VIIRS channels.

The VIIRS Imagery resolution bands 'nest' in the radiometric bands as is depicted in Figure 8.

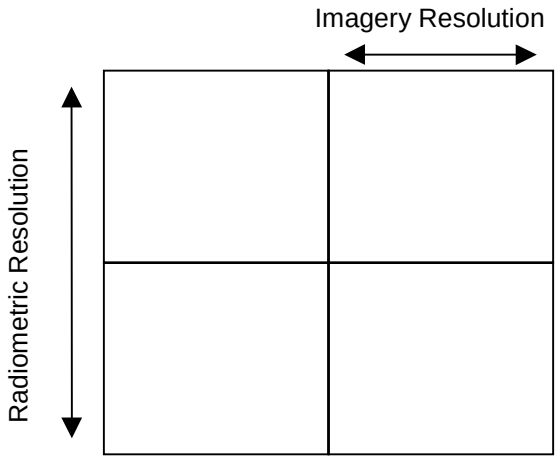

Figure 8. Depiction of the Nesting of the VIIRS Imagery Resolution Bands within the VIIRS Radiometric Resolution Bands

This nesting allows the inclusion of an imagery resolution cloud mask along with the VCM output. The individual imagery resolution pixels, 4 of which are contained within a given radiometric pixel undergo cloud detection tests, and the 2x2 imagery pixel region have spatial contrast tests done to them which are CLAVR heritage. For the 48 bit output IP the 4 bits are ordered from the upper left imagery resolution quadrant. The first bit is this upper left quadrant, the second bit is the upper right quadrant, the third bit is the lower left quadrant, and the fourth bit is the lower right quadrant.

3.2.2 Other Ancillary Data that *May* Prove Useful

The non-VIIRS data that may prove useful for the VCM is summarized in Table 5. This data is not required by the VCM.

Table 5. Ancillary non-VIIRS data for the VCM.

Input data	Source of Data
OMPS radiances	OMPS
OMPS EDRs	OMPS
CRIS radiances	CRIS
CRIS vertical EDRs	CRIS
CMIS radiances	CRIS
CMIS EDRs	CRIS

3.2.2.1 OMPS Radiances

Radiances from the OMPS instrument may improve cloud detection. The bands for the OMPS instrument are unknown to the VIIRS Integrated Project Team (IPT). It is assumed that the OMPS bands will be located in the ultraviolet (UV) spectral region. The use of OMPS bands needs to be investigated to determine their utility in the detection of high Polar Stratospheric Clouds (PSC). The PSC are sub-visual and are not detectable with VIIRS bands. Both the nadir and limb scanning instruments of the OMPS may be useful for cloud detection.

3.2.2.2 OMPS EDRs

OMPS EDRs may be useful for cloud detection in the VCM. The OMPS EDRs of Total Ozone, Ozone Profile, Tropospheric Ozone, Ozone Profile, and Aerosol Absorptance Index could be used to adjust the thresholds of UV cloud detection techniques reliant upon OMPS UV radiance measurements.

3.2.2.3 CRIS Radiances

CRIS Radiance data may be useful for cloud detection in the VCM. These data might be used in those platforms on which a CRIS and VIIRS instrument coexist. The use of the CRIS radiance data (for all three bands), needs to be investigated for the potential to improve cloud detection techniques. The nighttime cloud detection capabilities might benefit most from the CRIS data. MODIS investigations are presently underway with MODIS Airborne Simulator (MAS) data. Richard Frey, at the University of Wisconsin (UW), has in the past used the 13 micron channel in the MCM to demonstrate the utility of the radiances in the CRIS channels.

3.2.2.4 CRIS Vertical EDRs

Measurements of vertical temperature, pressure, and water vapor may improve the capabilities of the VCM. These profiles are modified in the presence of a cloud. Knowledge of water vapor profiles may assist with setting cloud detection thresholds for thin cirrus cloud detection tests at 1.375 microns, and other cloud detection tests. Knowledge of the amount of liquid water and ice in the atmosphere may assist cloud phase determination as well.

3.2.2.5 CMIS Radiances

Use of CMIS radiance data may improve cloud detection capabilities of the VCM, particularly at night. Passive microwave measurements over cloudy areas vary from those over clear regions. The amount of liquid water and ice in the atmosphere may be determined with CMIS data. This would directly assist in cloud detection.

3.2.2.6 CMIS Atmospheric Profiles

The value of atmospheric profiles has been mentioned previously for the CRIS vertical EDRs. Using CMIS atmospheric profiles may improve cloud detection.

3.3 THEORETICAL DESCRIPTION OF THE CLOUD MASKING

In the following section, the mathematical background of the processes outlined in Section 3.1 will be described. These processes only apply to regions which successfully passed the quality examinations.

3.3.1 Physics of the Problem

The detection of clouds using simple visible reflectance and thermal BT thresholding tests has been demonstrated with considerable success. Due to their nature, clouds are generally characterized by a higher surface reflectance and lower temperature than the underlying surface. This statement is generally true for most surface types around the Earth, such as ocean and sea level vegetated land. However, some surfaces require adjustments to the thresholds needed to detect clouds, and the use of different cloud detection tests. The various cloud detection tests and techniques will be discussed in the section below.

3.3.2 Pixel Level Cloud Detection Tests Presently Performed by the VCM

The basis of the VCM is the pixel level cloud detection tests. These are performed over an entire image. The pixel level tests define if a pixel is clear or cloudy. This will be done at the radiometric resolution using the radiometric channels, and at the higher imagery resolution using the imagery bands. Table 6 displays the current threshold values for the various cloud tests presently being performed within the VCM, note however the threshold values illustrated are for MAS channels, not VIIRS. As a result these threshold values are subject to change in the future, however the changes are not expected to be significant. The number of tests and scenarios will also increase with the development of the VCM. In the following section the various cloud tests currently employed are discussed, along with those which will be researched/considered in the future. Many of the tests presented here are performed by the MCM and CLAVR. Thresholds for the tests will be developed using MAS data sets.

In the future, contrast tests will be developed using the 2x2 imagery pixels which nest within the radiometric pixels to define clear and cloudy regions. These high-resolution tests will use imagery resolution channels, which are nested within and at a finer physical resolution than the VIIRS bands. Many of the techniques presently used by CLAVR will be used in contrast tests over the imagery pixels for cloud detection.

Table 6. VCM tests performed with MAS thresholds noted.

Test	Day Ocean	Night Ocean	Day Land	Night Land	Day Snow	Night Snow	Day Desert	Night Desert
BT11 IR Threshold	<270 K	<270 K	Not Used	Not Used	Not Used	Not Used	Not Used	Not Used
R1.38 High Cirrus	>2.5%	Not Used	>3.5%	Not Used	>3.5%	Not Used	>3.5%	Not Used
BT3.7–BT12 Thin Cirrus	Not Used	.6 K	-16K	>4.0 K	Not Used	>4.0 K	Not Used	Not Used
BT11–BT3.7 Low water clouds	<-8.0 K	>0.6 K	<-16.0 k	>0.6 K	>9 K	>0.6 K	Not Used	Not Used
R0.66 Visible reflectance test	Not Used	Not Used	>27%	Not Used	Not Used	Not Used	Not Used	Not Used
R0.87 Visible reflectance test	>7%	Not Used	Not Used	Not Used	Not Used	Not Used	>30 %	Not Used
R0.87/R0.66 Visible ratio test	0.9–1.1	Not Used	0.9–1.1	Not Used	Not Used	Not Used	Not Used	Not Used
BT3.7 – BT4.05 Cloud Detection Test	>6K	Not Used	>10K	Not Used	>8K	Not Used	Not Used	Not Used
R1.6 Near-IR reflectance test	>25%	Not Used	>50%	Not Used	>35%	Not Used	>60%	Not Used
BT8.6–BT11 & BT11–BT12 Tri-spectral cloud test	Table or <0.2 K	Table or <0.2 K	Table or >3.0 K	Table	Not Used	Not Used	Not Used	Not Used

Note: These values are developed from representative MAS spectral data.

3.3.2.1 BT11–Test

This BT threshold test is a simple IR window threshold test. This test is performed over open water. The test should be cautiously used in other regions, due to the effects of cold snow/ice surfaces upon this channel, and the emissivities of some land types. Over open ocean, when the BT of the 11 micron channel is less than 270 K, the pixel is detected as cloudy. This test is only applied over open water at present. However, the use of this test over various surface types will be investigated.

3.3.2.2 BT3.7–BT12–Test

Applying this BT difference test is useful for separating thin cirrus and cloud free conditions (Hutchinson and Hardy, 1995).

3.3.2.3 BT11–BT3.7–Test

This test became best known for the detection of stratus in nighttime imagery (Saunders and Kriebel, 1988); however, this BT difference test is also useful for detecting clouds both day and night. The differences present in a cloudy scene are a result of the different emissivity between the 3.7 and 11 micron channels, and the presence of a solar component in the 3.7 micron channel. Thermal difference tests will be performed with caution in the polar regions, where cold surface temperatures may give false cloud detection.

3.3.2.4 BT8.6–BT11 and BT11–BT12

The spectral uniformity of surface emittance in these IR window regions can be used to detect clouds. For a complete explanation of the technique see Ackerman *et al*. (1990) and Strabala *et al*. (1994).

3.3.2.5 R.66 Test

A single channel reflectance test for bright clouds over dark surfaces may be applied using the 0.65 micron channel. This test may not be used over bright snow/ice covered surfaces, but has success over heavily vegetated and open ocean regions.

3.3.2.6 R.86 Test

A single channel reflectance test for bright clouds over dark surfaces may be applied using the 0.86 micron channel. This test may not be successful over vegetated regions, but has demonstrated some success over snow/ice and desert regions.

3.3.2.7 R.86/R.65 Test

This reflectance ratio test is based upon the fact that the reflectances for cloud covered regions in these bands should be very close to one another (Saunders and Kriebel, 1988). For cloudy pixels, this ratio is slightly less than 1, but may be as small as 0.6 depending upon solar illumination and scattering geometry. But over clear vegetated land scenes this ratio is generally greater than 1, and for clear water surfaces this ratio is much less than 1, depending upon solar illumination and scattering geometry (Hutchinson and Hardy, 1995).

3.3.2.8 R1.38 Test

A single channel reflectance test for high cirrus clouds (Gao *et al*., 1992; Gao *et al*., 1993). This single channel reflectance test greatly improves the detection of thin cirrus over land surfaces in daytime imagery, if sufficient lower-level water vapor is present (Hutchinson and Choe, 1996) and can be used to decouple high cirrus clouds from lower level clouds for the analysis of cloud top phase (Hutchinson, 1997). The high amount of water vapor absorption across this channel means the surface and lower level cloud reflectance is absorbed by water vapor. The resulting reflectance signature is indicative of a thin cirrus cloud presence. This test may require modifications to the thresholds, if it is to be applied in polar regions with low water vapor levels.

3.3.2.9 R1.6 Test

This test uses the high absorption of snow/ice surfaces, and the high variable reflectance of clouds within this band to differentiate between water clouds and these cloud-free surfaces (Valvocin, 1978). The test has demonstrated promising capabilities for cloud detection over snow and sea ice, and cloud vs. snow/ice discrimination.

3.3.2.10 BT3.7 - BT4.05 Difference Test

Doing this BT difference test is another method of removing the solar and thermal contribution of the 3.7 channel. Due to the small wavelength differences between these two bands the thermal contribution due to temperatures within a pixel are relatively close. The largest difference between these two bands is the solar component in the 3.7 channel. The difference removes the BT resulting from the solar component of 3.7 alone. Due to both the low reflectances of most surface types, and the relative high reflectance of clouds in the 3.7 channel this test has demonstrated much promise in MAS data.

3.3.2.11 Imagery Band Tests

The imagery bands on the VIIRS sensor are at a finer resolution than the other VIIRS radiometeric bands, which they nest within. Presently they are assumed to be bands centered at 0.65, 0.86, 1.6, 3.7, and 11.45 microns, and to have a HCS of approximately 370 meters. Cloud tests performed with these bands will reported at the imagery resolution, and have spectral contrast tests performed upon them, along with tests being performed at the finest resolution they offer. These tests performed are BT and reflectance tests of CLAVR heritage.

3.3.2.12 BT11–Test

This BT threshold test is the same as the test used for the radiometric test, but uses the Imagery resolution band centered at 11.45 microns.

3.3.2.13 BT11–BT3.7–Test

This BT difference test is the same conceptually as the test used at the radiometric resolution with the radiometric bands, but it is performed at the imagery resolution with the imagery bands centered at 3.7 and 11.45 microns.

3.3.2.14 R.66 Test

This Reflectance threshold test is the same as the test used for the radiometric resolution test, but uses the Imagery resolution band centered at .645 microns.

3.3.2.15 R.86 Test

This Reflectance threshold test is the same as the test used for the radiometric resolution test, but uses the Imagery resolution band centered at .845 microns.

3.3.2.16 R.86/R.65 Test

This reflectance ratio test is the same as the test used for the radiometric resolution test, but uses the Imagery resolution bands centered at .645 and .845 microns.

3.3.2.17 R1.6 Test

This reflectance ratio test is the same as the test used for the radiometric resolution test, but uses the Imagery resolution band centered at 1.6 microns.

3.3.3 Cloud Detection Tests Recommended for further Investigation

3.3.3.1 BT8.6–BT3.7–Test

This would be a radiometric resolution pixel threshold based test. This test has shown promise in detection of clouds over snow and ice covered surfaces, it is under investigation.

3.3.3.2 BT3.7 Thermal and Solar Component Separation Tests

By decoupling the solar and thermal component of the 3.7 micron channel, it has been demonstrated that the contrast between snow-covered surface and thin cirrus is greatly enhanced using only the reflective characteristics, along with the AVHRR 0.6 micron band (Allen *et al*., 1992; Hutchinson *et al*., 1997; Hutchinson and Locke, 1997). Also, there is similar behavior of the complex component of the indexes of refraction of ice and liquid water between this channel and the 1.6 micron channel. For this reason, the solar components reflectivity may be used to perform similar reflectance tests as those which are planned with the 1.6 micron channel above. This will be investigated at Raytheon using simulated and MAS data.

3.3.3.3 DNB Test

The VIIRS DNB may be useful for non-polar region cloud detection at night when lunar illumination is concurrent. Use of this DNB may also be useful over urban regions where clouds should obscure city lights. An imagery resolution cloud detection threshold needs to be developed using the DNB reflectance. The methodology for this would be the same applied over the other imagery resolution bands. Also Contrast tests may be developed with this DNB using the 2x2 DNB pixels nested within any radiometric pixel.

3.3.3.4 Imagery Resolution Contrast Tests

The VIIRS Imagery resolution pixels may be used for contrast using the 2x2 DNB pixels nested within any radiometric pixel. These tests would be CLAVR in heritage and assist greatly in sub-radiometric resolution pixel cloud detection.

3.3.4 Pixel Level Additional Tests

3.3.4.1 Non-Cloud Obstruction Test

Detection of non-cloud aerosols are important for the cloud mask, for those sun/sensor geometries which create long path-lengths. For long path-lengths, aerosol-laden atmospheres may be misinterpreted as clouds by some tests. This is due to the enhanced reflectances in the visible bands created by the non-cloud obstructions. This test is present primarily for the Imagery Analyst to assess the presence of aerosols by use of an automated indicator. To detect aerosols in the path, simple pixel level tests are planned. A quality flag indicating the performance will be output from the cloud mask. Presently, the plan is to use tests involving the 11 and 12 micron VIIRS channels to detect the presence of dust storms. Similar tests will identify heavy aerosol using the 2.1 and the 0.65 micron bands. In addition, it is possible that a simple fire detection test will be employed using the 3.7 and 11 micron channels.

3.3.4.2 Cloud Shadow Test

Detection of cloud shadows is a problem which has not been addressed adequately in the literature. Some approaches perform a theoretical computation of shadows from viewing geometry, solar azimuth and zenith angles, cloud edge distribution, and cloud top altitudes. But these approaches require far too much computation time to run operationally. The current VCM cloud shadow detection approach is the MODIS shadow detection approach. This only works over vegetated regions. Cloud-on-cloud shadows will not be detected by this algorithm. Topographical shadowing may be investigated, if time permits, and when DEMs evolve to include parameters to investigate such effects.

3.3.4.3 High and Low Cloud Test/Flags

These two cloud Flags are indicated when a test which is indicative of a high or low cloud is triggered. The reason for these flags is that they may be used by the Cloud Cover/Layers to indicate a multi-layered cloud and also by the Cloud EDRs which follow in the processing architecture. They also can aid in cloud phase assessment.

Detection of single versus multi-layered clouds is done once all of the cloud mask tests have been performed on a pixel. By looking at the cloud tests results one can infer the presence of a possible multi-layered clouds presence. This is due to some cloud tests detecting the presence of high clouds only, while others are sensitive to low clouds presence. The results of this test are useful to an analyst and will benefit the Cloud Cover Imagery EDR.

3.3.4.4 Cloud Phase Test/Flag

The VIIRS Cloud Phase Algorithm determines if a pixel, which has been classified as cloudy by the VIIRS Cloud Mask, contains a cloud which is composed of predominantly water or ice particle phase. To perform cloud phase determination the VIIRS radiance data for channels.645, 0.859, 1.375, 1.61, 3.75, 8.6, 10.8, and 12.0 microns are used along with additional ancillary data. This Cloud Phase Testing is presently done in the VCM, but in need of refinement in the future.

The ancillary data required as input to the cloud phase determination algorithm are a global land/sea map, ecosystem map, sun/sensor geometry, and snow/ice map

The VIIRS Cloud Phase (VCP) SDR is developed from a hybrid of the MODIS, AVHRR, and GOES Cloud Phase detection techniques. In being a hybrid algorithm it utilizes the best cloud phase determination features from all of these cloud phase assessment and algorithmic techniques. The overall processing structure is a direct result of a modularized flow which is expected to decrease both necessary processing time and efficiently determine cloud phase.

Generation of the Cloud Phase occurs routinely within the VCM as part of the first level of EDR processing. The Cloud Phase pixel level results are then used at a pixel level by the other Cloud EDRs. Results of the Cloud Phase algorithm will define the pixel as containing a cloud which is predominantly water, ice, or undetermined. Figure 9 illustrates the VCP algorithm and a discussion follows.

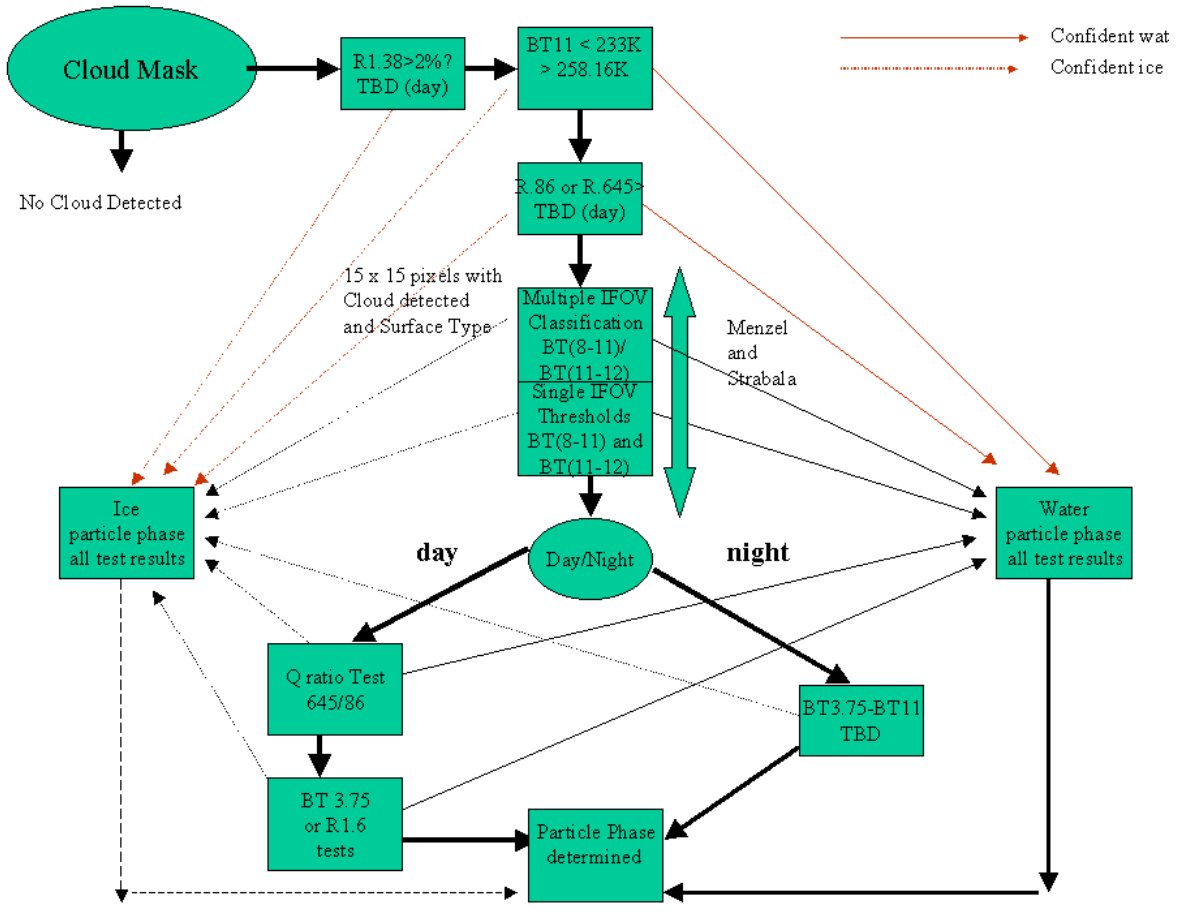

Figure 9. VIIRS Cloud Phase Algorithm (Contained within the VCM)

The first preprocessing step, which is depicted in the VCP algorithm, in Fig. 1 above, is the determination by the VCM if a cloud is present. For clear pixels the VCP algorithm will not be executed. In addition to the pixel being detected as cloudy, knowledge of the underlying surface type, sun/sensor geometry, if the pixel is in the day or night regime, and the reflectance's and BT's of bands used by the VCP are required as input.

Following the indication by the VCM of a clouds presence in the pixel region the first three thresholding tests are the confident indicators of cloud particle phase. If a pixel's cloud phase is indicated by one of these first three tests then its phase will not be changed as a result of tests which are performed later in the VCP algorithm. Only those pixels whose phase is undetermined by the first three tests will be designated by tests done afterwards in the VCP algorithm. These first three tests are the R1.38, BT11, and visible/NIR reflectance thresholding tests. These tests are as follows:

The reflectance at 1.38 microns being greater than (TBD 2%) is indicative of a high cirrus being present. The basis for this is that the large water vapor absorption in this band causes lower level reflected light to be absorbed, leaving the reflected light which is measured by the sensor only reflected light from high cirrus clouds. This phase test would only be done during the day, and would indicate ice phase only.

The BT 11 microns test is to be done day and night. For BT11 < 233 K the ice particle phase is indicated, while for BT > 258.16 K (TBD) the water phase is indicated.

The R 0.86 and R 0.645 tests are reflectance tests based upon the reflectance of the clouds. For ice clouds the reflectance in both of these bands is less than water clouds, and for water clouds the reflectance in these bands is large. The 0.645 band will be used over land, while the 0.86 band will be used over water, due to the large reflectance of vegetated surfaces at 0.86. Values for the phase indicating thresholds are TBD presently, however there will be ranges of uncertainty and an angular dependence for these tests. This will be a daytime only test.

In Figure 9 the dashed red lines indicates that this is a final decision that the cloud phase is indicated and the phase classification is complete. However, the pixels thus classified are still used in the 15x15 pixel aggregation for Menzel and Strabala's tests. This is due to a need for enough pixels of defined ice type being needed to allow a defined slope for the Multiple IFOV Classification step. Those which have been classified by preprocessing tests are not reclassified a second time by the VCP algorithm, however the results of the multiple tests following are flagged and may be used at a future point to indicate problems with tests performed our define phase irregularities.

Once the three initial cloud phase tests are performed, and a 15 x 15 matrix of determined and undetermined cloud phase pixels are collected then the Menzel and Strabala tests will be performed, this is performed in a two step algorithm scheme.

The first step is a Multiple IFOV Classification of the 15x15 matrix of pixels. This step considers the slope of the BT(8-11) vs. BT(11-12) plot and determines the pixels which have dominant clustering of about a common slope. This is developed from Menzel and Strabala's MODIS work. For the slope defined as BT(8-11)/BT(11-12) the pixel phase is defined as ice for slopes > 1.0 (TBD) and water for slopes < 1.0 (TBD). The results in the pixel matrix are flagged based upon their clustered slopes, and those pixels which are not clustered are not flagged.

The second step is the Single IFOV Characterization of the 15x15 pixel matrix. This step uses a threshold approach to define the cloud phase. For BT(11-12) > 1.5 K and BT(8-11) < 1.5 K (TBDs) the cloud phase is determined to be ice. While for BT(11-12) < 1.5 K and BT(8-11) > 1.5 K (TBDs) the cloud phase is ice.

For those pixels which still do not have their phase determined additional tests will then be performed. Those tests are the Q ratio test and additional thresholding tests which employ the 1.6 and 3.75 bands that are under development at RITSS, during the day. During the night one additional BT(3.75-11) test will be performed to detect ice clouds, this is a threshold test and the value is TBD. These tests are under development.

Results of the various tests of the Multiple IFOV classification, Single IFOV Characterization, and the threshold tests that follow are all then compared, and the decision of the final phase distinction is then performed. For cases in which there are tests that indicate both ice and water the pixel will be flagged as a possible mixed phase, and for pixels with no cloud phase indicated the pixel will be flagged as unknown.

Once the cloud phase is determined it is output as part of the VCM output to the other EDRs. The knowledge of cloud phase will allow more accurate indexing of the Look Up Tables (LUT) used to retrieve the Cloud Optical Thickness and the Cloud Effective Particle Size EDRs.

3.3.4.5 Sun Glint Test

Sun glint pixels possess glitter contamination. Consequently, the pixels in which possible sun glint is occurring need to be identified. Solar channel threshold values need to be adjusted for these pixels. Sun glint will not result in a cloud mask being generated. In the case of sun glint the solar tests performance may be inhibited, but the thermal channel tests will still be done to generate the equivalent of a nighttime cloud mask. Knowledge of sea surface winds may be included in the sun glint test, surface winds can narrow the region in which sun glint may occur. There is a justifiable concern that cloud detection will not be as reliable in glitter-contaminated regions. A classification as clear is probably correct, but a classification as cloudy may actually be due to the glitter effect as opposed to a cloud. Sun glint will be considered over both land and water areas. Land regions are included because spatially unresolved water bodies, snow, or recent rainfall can also cause sun glint.

Sun glint may occur when the reflected sun angle θ_r, is 0° to 36°, where:

$$\cos\theta_r = \sin\theta \sin\theta_o \cos\phi + \cos\theta \cos\theta_o \quad (1)$$

Where θ_o is the solar zenith angle, θ is the viewing zenith angle, and ϕ is the azimuthal angle.

Sun glint is also a function of surface with and the state of the ocean, and effected by sea surface winds. In the future these parameters will be considered in sun glint pixel identification within the cloud mask, presently these are not considered. This output will be used by the Ocean EDRs to identify sunglint regions.

3.3.4.6 Automated Fire Detection

This will follow the MODIS methodology and will be activated in the future, it may result in additional bands being required as input into the VCM. The author believes that the bands of use for this work are already being used by the VCM.

3.3.5 Cloud Mask Over Varying Surfaces

Cloud masking over varying surface types requires the use of different thresholds to be applied over the different surfaces. The pixels are classified within a specific region based upon their geolocation, day/night, land/water, and other categories. The pixel level thresholds being applied over the regions presently considered are shown in Table 5. As the VCM evolves, additional regions may be added to improve the results of the cloud mask. New thresholds for specific regions will be developed.

3.3.5.1 Cloud Mask Over Land

A conceptual flow of the cloud mask algorithm performed over land surfaces is illustrated in Figure 10. This occurs after a pixel has been identified to be within a land region (Figure 7). The pixel is first classified as day or night. For the purposes of the cloud mask, “day” is defined as when the solar zenith angle of the pixel is less than 85 degrees. Greater solar zenith angles are considered as “night.” After designation of day land or night land, the snow/ice detection is applied. Presently, the land type is only subdivided into vegetated land and desert ecosystems. In the future, it is expected that the number of different ecosystems considered will increase. Vegetated land surfaces have spectral reflectances such as displayed in Figure 11. From these spectra, one can see the low reflectance in the visible, and higher reflectance in the near IR region. Table 5 displays the cloud tests which are performed over the vegetated land surface type and the thresholds presently being applied.

VIIRS DECISION TREE FOR LAND REGION

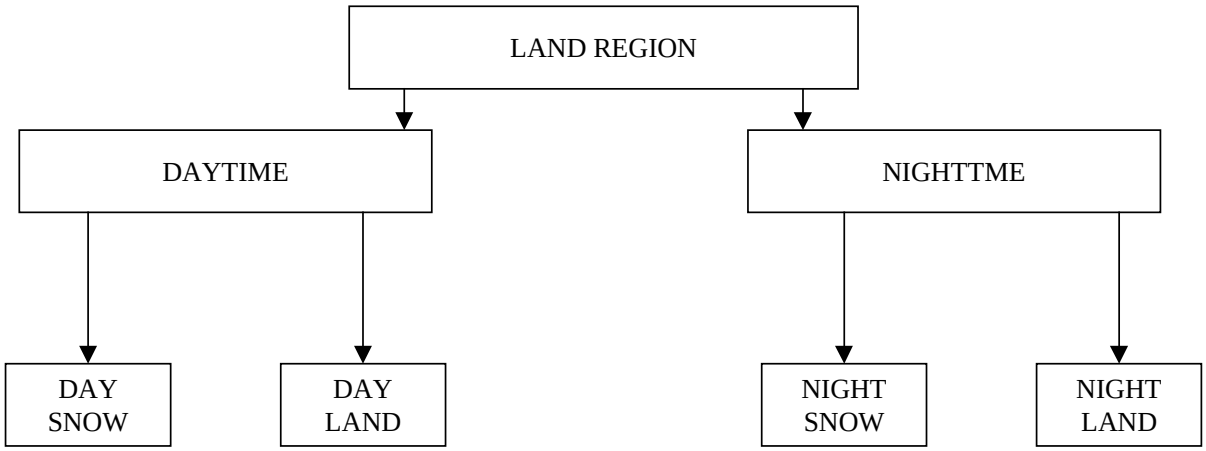

Figure 10. Conceptual flow of the VCM over coastal regions.

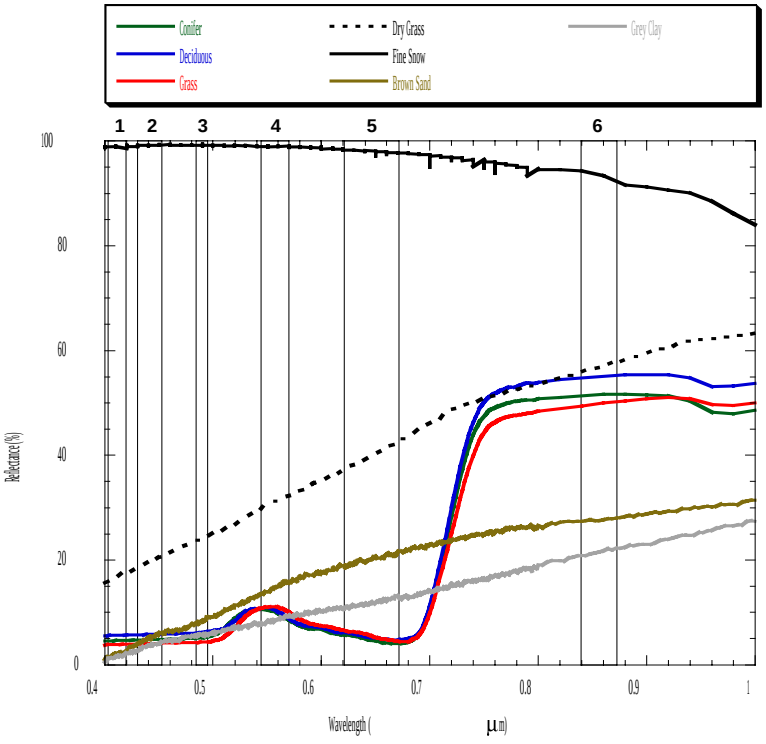

Figure 11. Laboratory measured spectra for several land cover types from 400 to 1000 nm. VIIRS nominal bands 1 through 6 are approximately shown as numbered boxes. (Spectra are available through the ASTER spectral library http://speclib.jpl.nasa.gov).

3.3.5.2 Cloud Mask Over Coastal Regions

Pixels in the regions between the land and water are classified as coastal regions. Figure 12 illustrates the decision tree flow for a coastal region. As was done previously, the classification is subdivided into day and night. Then the scene is further classified into either day snow, day coastal, night snow, or night coastal. The coastal region is designated as a separate subregion due to cloud classification problems which are likely to occur over coastal areas. Within coastal regions, the confidence of the cloud mask will be assumed to be lower than for other regions. Thresholds for this region are shown in Table 5 as well. Presently the Coastal Region thresholds have not been developed for the VCM. In the future the MCM approach will be reviewed to determine if their thresholds are of use in the VCM.

3.3.5.3 Cloud Mask Over Water

Pixels which are designated as water follow the conceptual flow shown in Figure 13. The water surface region is subdivided into day and night cases, and then further subdivided into snow/ice covered surfaces. Water surface reflectances are shown in Table 7, from the NPOESS Toolkit. The reflectance is uniformly low across the spectrum. As a result of this low reflectance for water surface, the detection of highly reflective clouds is expected to be very successful. Another beneficial property of water surfaces is that the temperature of water must be greater than 270 K. This allows BT tests to also be more successful. The thresholds for cloud detection over water are shown in Table 6.

VIIRS DECISION TREE FOR COASTAL REGION

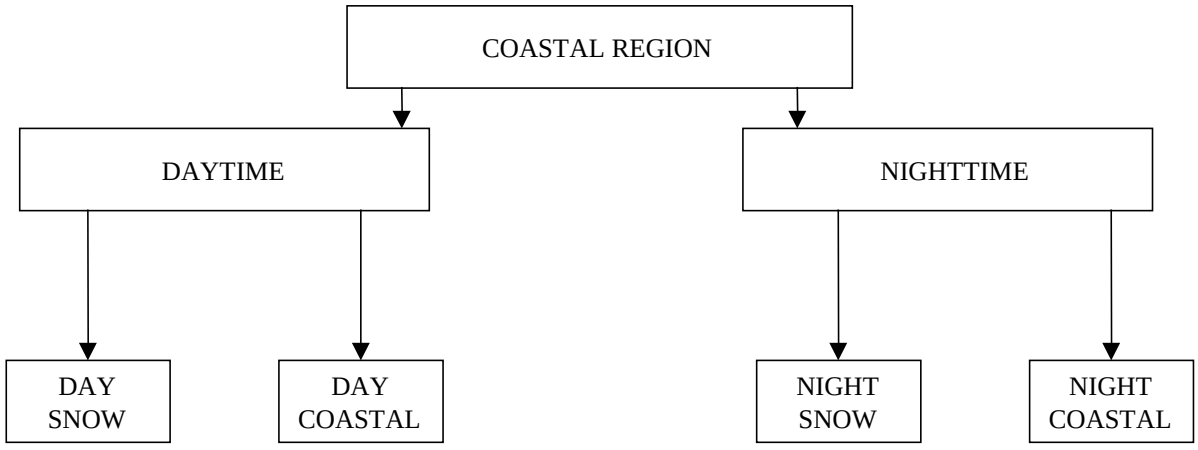

Figure 12. Conceptual flow of the VCM over coastal regions.

VIIRS DECISION TREE FOR WATER REGION

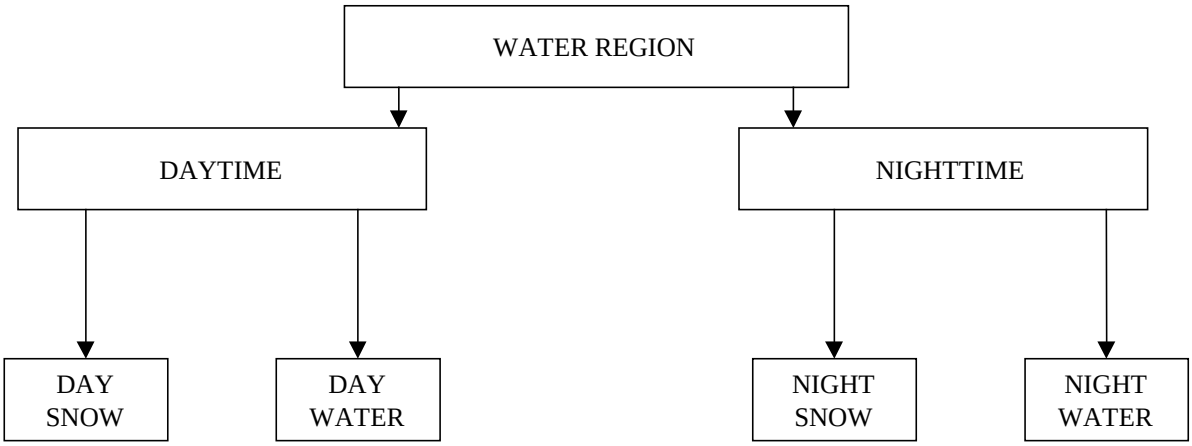

Figure 13. Conceptual flow of the VCM over water regions.

Table 7. Spectral Reflectances Being Used in Cloud Simulations to Develop the VCM

Band (μm)	Desert	Water	Broadleaf Forest	Old Snow	New Snow
0.65	0.46	0.005	0.014	0.889	0.969
0.86	0.506	0.007	0.3155	0.642	0.912
1.2	0.565	0.024	0.444	0.164	0.654
1.38	0.60	0.024	0.310	0.094	0.516
1.61	0.64	0.023	0.260	0.000	0.158
2.12	0.66	0.016	0.032	0.002	0.08
3.75	0.45	0.020	0.043	0.013	0.023
8.5	0.10	0.01	0.038	0.009	0.009
10.8	0.02	0.01	0.038	0.008	0.01
12	0.02	0.01	0.050	0.018	0.018

3.3.5.4 Cloud Mask Over Polar Regions

Regions which are located north of 36 degrees or south of 50 degrees latitude are designated as polar regions. For pixels in the polar region a conceptual flow is shown in Figure 14. The latitudinal extent of the polar regions is defined based on the historical range that sea ice is found in the ocean, or where ice covers land. The complexity of the classifications for polar regions is displayed in the conceptual flow diagram. Another aspect of the polar regions is the decreased amount of atmospheric water vapor present, relative to other regions of the Earth. This may require modified thresholds to be applied to the R1.38 tests, which are sensitive to the amount of atmospheric water vapor.

3.3.5.5 Cloud Mask Over Snow/Ice regions

The spectral reflectance for snow-covered regions is shown in Table 7. Cloud detection over snow/ice covered regions are the most difficult. Each of these surfaces have a high reflectance in the visible combined with a low surface temperature. These traits lead to common confusion/misclassification with clouds, so cloud detection can be difficult. The confidence of cloud detection in such regions will be low. The thresholds applied across snow/ice covered regions is shown in Table 6. As is apparent from this table, the number of tests done in the case of a snow/ice covered region is quite limited, this is a direct result of the reflectance and temperature traits of snow and ice.

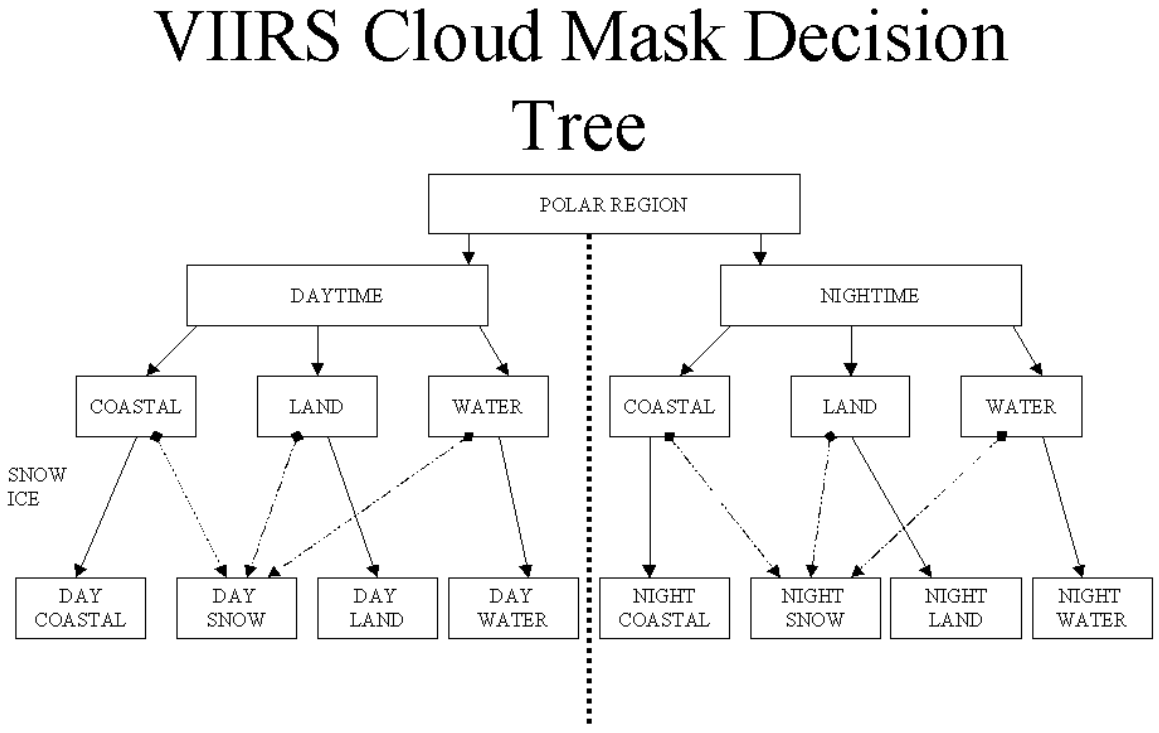

Figure 14. Conceptual flow of the VCM over polar regions.

3.3.5.6 Conversion From Cloud Mask to Cloud Fraction

Cloud cover will be an aggregation over a pixel region of the cloud mask cloudy/not cloudy results. Summing these results over a given area and dividing by the total number of pixels within that area will result in the fractional cloud cover. The HCS at which this will be done is still being considered. The cloud mask will deliver the cloudy/not cloudy decision at the radiometric and imagery pixel levels.

This section will be expanded upon following the work of Bretherton and Coakley (1983) and the VIIRS Cloud Cover/Layers ATBD [*V-8*].

3.3.6 Archived Algorithm Output

The output will be a binary result (1's and 0's) for each pixel. The exact number of bytes for each pixel of output is presently 6, but may be increased as needed. This is dependent upon the number of cloud tests performed in the final product, and the demands placed upon the cloud mask by other VIIRS EDRs. The 48 bit output is summarized in Section 3.1.

3.3.7 Error Budget and Misclassification Estimates

The concept of automated cloud detection in multispectral imagery, used to generate the automated cloud mask, is based upon a robust methodology which employs a series of tests that exploit the spectral signatures of ice and water clouds. This methodology is robust because clouds that may not be detected by one single test, described in Section 3.3.2 and 3.3.3, will generally be detected by another. Often, clouds are detected by multiple tests. This redundancy in cloud detection tests provides assurance that clouds will not fail to be detected even as the VIIRS sensor or ancillary data become degraded with time or circumstances, e.g., ancillary data are not available. However, due to the binary nature of a cloud mask, being cloud/no cloud the terms of Accuracy and Precision cannot readily be used to construct an error budget for the cloud mask. The misclassification of the cloud mask is being used to assess the performance of the VCM.

One is unable to assess the performance of the cloud mask in terms of accuracy and precision requirements that are defined by the SRD for the Cloud Cover/Layers EDR, misclassification of the cloud mask is thereby defined. Misclassification is the percentage of pixels within a given scene that are classified as cloudy when clear or clear when cloudy. The rationale behind this subdivision of the misclassification is the fact that each case of misclassification will effect different EDRs in varying ways. For demonstrations of the misclassifications refer to the Cloud Mask flowdown documents. Subdivision into the two misclassifications, cloudy when clear and clear when cloudy, is important because the misclassification of clear when cloudy will effect VIIRS surface EDRs, while the misclassification of cloudy when clear will effect the cloud EDRs. The goal of the cloud mask algorithms development is to minimize the misclassification amount. The probability of correct typing of the VCM is one minus the total misclassification.

With the cloud mask being evaluated based upon misclassification, a plan has been devised to evaluate the impact of system-level errors on the automated cloud mask product in terms of misclassification in order to determine which, if any, are system drivers. The procedure uses numerous simulations of VIIRS imagery under different levels of degradation, described below.

Automated analyses of simulated imagery are then compared against ground truth cloud masks used to generate the simulations as described in the VIIRS Imagery ATBD [*V-1*] (Topping *et al*., 1998). These pixel-level comparisons between the automated cloud mask and the ground truth cloud mask have proven useful for quantitative analyses required for error budget (VIIRS Imagery ATBD [*V-1*], 1998; Hutchison *et al*., 1997; Hutchison and Choe, 1996; Hutchison and Hardy, 1995; Hutchison *et al*., 1995). While this work is ongoing, a theoretical description of the errors which will be evaluated is provided.

The total misclassification in the Cloud Mask product can be estimated as:

$$M_{tot} = 1 - \left((1 - M_{geo}) * (1 - M_{BBR}) * (1 - M_{dyn}) * (1 - M_{NEdL}) * (1 - M_{alg}) * (1 - M_{rad\_acc}) \right.$$
$$\left. * (1 - M_{anc}) * (1 - M_{alg}) * (1 - M_{bb}) \right) \qquad (2)$$

While one can divide the total misclassification down into its two terms of cloudy when clear (M1) and clear when cloudy (M_2) as follows:

$$M_{tot} = M_1 + M_2 \qquad (3)$$

At present, the interacting effects of the ensemble of error sources are thus not yet clear and are thus hard to assess. Therefore, the error sources have initially been assumed to be independent in their contribution to cloud misclassification. Further studies on this topic are necessary. In the following subsections, the different error sources will be investigated separately .

The Probability of Correct Typing, which is used in assessment of the Cloud Mask performance is as follows:

$$P_{tot} = 1 - M_{tot} \qquad (4)$$

This is a measure of the total probability of correct typing.

3.3.7.1 Errors Due to Geolocation/regional Misclassification

Simulations of VIIRS radiances and imagery generated for erroneously classified regions and automated analyses of simulated imagery are then compared against ground truth cloud masks. This is considered to be an error source which contributes directly to the error in surface type.

3.3.7.2 Errors Due to Band-to-Band Registration

Simulations of VIIRS radiances and imagery generated with band-to-band registration errors of different degrees, e.g., ¼ from 0-60%pixel misregistration, and automated analyses of simulated imagery are then compared against ground truth cloud masks used to generate the simulations. A Band-to-Band Registration study is ongoing. Results of Band-to-Band Misregistrations effects have shown that band-to-band RMS misregistrations greater than 20% can lead to misclassifications of greater than 10%. Also, band-to-band misregistration effects the clear when cloudy misclassification much more than the cloudy when clear misclassification. This behavior is believed to be due to the cloud conservative behavior of the cloud mask itself. For example the ratio of clear when cloudy to cloudy when clear misclassifications is roughly equal for band-to-band misregistrations less than 20%, but as misclassification increases beyond 20% results have shown that the ratio goes as high as 7:1. High amounts of band-to-band misregistration have their largest effects upon surface EDRs, which are determined when a cloud is not detected. Among these surface EDRs are CAT-1 EDRs, which have the highest importance placed upon them by the IPO. Therefore, it is recommended that band-to-band misregistration be kept less than 20%. See Flowdown Document SPAT.BBR.VCM for these results.

3.3.7.3 Errors Due to Sensor Noise

Results are in Flowdown Document RAD.NEDL.VCM.

Simulations of VIIRS radiances and imagery were generated with different sensor noise models and automated analyses of simulated imagery were then compared against true cloud fields used to generate the simulations.

3.3.7.4 Errors Due to Surface Type Misclassification

Presently the Ecosystem and Land/Sea Maps used by the VCM are the same as those used by MODIS. The MODIS team has considered these maps to have an accuracy of 1%. For the assessment of the size of this error it must be considered that surface type misclassification is minimal in the large homogeneous surface types of the earth, ie. minimal over the oceans and the vegetated land regions. The effect of surface misclassifications will be greatest in regions which possess snow/ice which is not known to be there. This is considered to be a small set of the total pixels which the VCM will map.

3.3.7.5 Errors in Continuity

Since many of the VIIRS bands resemble the MODIS bands, continuity with respect to the MODIS sensor is straightforward. With respect to bands which resemble AVHRR, the spectral and spatial aggregation requires further study.

3.3.7.6 Errors Due to the MTF

These errors were considered and found to be minimal, MTF does not play a large role in affecting cloud detection.

See Flowdown Document SPAT.BBR.VCM for use of the MTF.

3.3.7.7 Errors Due to Polarization

At this time, we assume the sensor to be a polarization insensitive instrument. We believe that ocean EDRs are more affected by this topic. (See instrument document.). In addition the bands used by the VCM are greater than .600 microns, as such it is believed that the effects of polarization will be minimized.

3.3.7.8 Errors Due to Out of Band Response

Experience with MODIS has indicated that some detectors are vulnerable to signals far outside their targeted spectral range (Out-of-Band Leakage). Additionally, any detector will have a spectral response that will include contributions from the immediately surrounding wavelengths, as the bandwidth itself is generally defined by selecting the full-width half-maximum (FWHM) of the spectral response curve. While the VCM will be affected, it is believed that these effects will be minimal.

3.3.7.9 Error Budget

An attempt has been done to assess the Cloud Mask error budget as defined in Equation 4 above. For the varying cases, values have been inserted either from flowdown results or from experience with the Cloud Masks capabilities. The Error Budget is shown in Table 8. In this table the performances are the lowest probabilities of correct typing for the Water and Land surface types considered. For a more stratified review of the Probability of Correct Typing refer to Table 10.

Table 8a. VIIRS Cloud Mask Error Budget

VIIRS CLOUD COVER (Binary Map)			OCEAN, DAYTIME		
Specification V3 (PDR)	Inputs		Probability of Correct Typing		Note that Probabilities do not RSS
March 21,2000	Error	Unit	$\tau < 1$	$\tau > 1$	References and Notes
Threshold			>(TBD) at (TBS)% confidence level		SRD V2, Rev a
Objective			>(TBD) at (TBS)% confidence level		SRD V2, Rev a
System Specification			91%	100%	Cloudy/not cloudy, VCM ATBD
System Performance			92%	99%	
System Margin			1%	-1%	
Algorithm Performance			98.0%	99.7%	total of algorithm errors
Surface Type misclassification	1	%	99.00%	99.99%	VCM ATBD
Land/water mask	50	m			In surface misclassification
DEM elevation	50	m			In surface misclassification
Intrinsic Algorithm Error			99.00%	99.70%	
Sensor Performance			93.9%	99.6%	total of sensor errors
Geolocation (3σ)	200	m	99.00%	99.90%	
NEdT	baseline		98.30%	99.90%	
Calibration	baseline		99.00%	99.90%	
MTF	baseline		97.50%	99.90%	
band to band misregistration	0.2	pixels			

Table 8b. VIIRS Cloud Mask Error Budget

VIIRS CLOUD COVER (Binary Map)			OCEAN, NIGHTTIME		
Specification V3 (PDR)	Inputs		Probability of Correct Typing		Note that Probabilities do not RSS
March 21,2000	Error	Unit	$\tau < 1$	$\tau > 1$	References and Notes
Threshold			>(TBD) at (TBS)% confidence level		SRD V2, Rev a
Objective			>(TBD) at (TBS)% confidence level		SRD V2, Rev a
System Specification			88%	100%	Cloudy/not cloudy, VCM ATBD
System Performance			91%	97%	
System Margin			3%	-3%	
Algorithm Performance			98.0%	99.0%	total of algorithm errors
Surface Type misclassification	1	%	99.00%	99.99%	VCM ATBD
Land/water mask	50	m			in surface misclassification
DEM elevation	50	m			in surface misclassification
Intrinsic Algorithm Error			99.00%	99.00%	
Sensor Performance			93.1%	97.8%	total of sensor errors
Geolocation (3σ)	200	m	99.99%	99.99%	
NEdT	baseline		97.00%	99.33%	
Calibration	baseline		99.00%	99.91%	
MTF	baseline		97.00%	98.53%	
band to band misregistration	0.2	pixels			

Table 8c. VIIRS Cloud Mask Error Budget

VIIRS CLOUD COVER (Binary Map)			LAND, DAYTIME		
Specification V3 (PDR)	Inputs		Probability of Correct Typing		Note that Probabilities do not RSS
March 21,2000	Error	Unit	$\tau < 1$	$\tau > 1$	References and Notes
Threshold			>(TBD) at (TBS)% confidence level		SRD V2, Rev a
Objective			>(TBD) at (TBS)% confidence level		SRD V2, Rev a
System Specification			85%	95%	Cloudy/not cloudy, VCM ATBD
System Performance			90%	97%	
System Margin			5%	2%	
Algorithm Performance			98.0%	99.0%	total of algorithm errors
Surface Type misclassification	1	%	99.00%	99.99%	VCM ATBD
Land/water mask	50	m			in surface misclassification
DEM elevation	50	m			in surface misclassification
Intrinsic Algorithm Error			99.00%	99.00%	
Sensor Performance			92.2%	98.3%	total of sensor errors
Geolocation (3σ)	200	m	99.00%	99.99%	
NEdT	baseline		97.00%	99.90%	
Calibration	baseline		99.00%	99.00%	
MTF	baseline		97.00%	99.40%	
band to band misregistration	0.2	pixels			

Table 8d. VIIRS Cloud Mask Error Budget

VIIRS CLOUD COVER (Binary Map)			LAND, NIGHTTIME		
Specification V3 (PDR)	Inputs		Probability of Correct Typing		Note that Probabilities do not RSS
March 21,2000	Error	Unit	$\tau < 1$	$\tau > 1$	References and Notes
Threshold			>(TBD) at (TBS)% confidence level		SRD V2, Rev a
Objective			>(TBD) at (TBS)% confidence level		SRD V2, Rev a
System Specification			82%	91%	Cloudy/not cloudy, VCM ATBD
System Performance			90%	91%	
System Margin			8%	0%	
Algorithm Performance			98.0%	99.0%	total of algorithm errors
Surface Type misclassification	1	%	99.00%	99.99%	VCM ATBD
Land/water mask	50	m			in surface misclassification
DEM elevation	50	m			in surface misclassification
Intrinsic Algorithm Error			99.00%	99.00%	
Sensor Performance			92.2%	92.2%	total of sensor errors
Geolocation (3σ)	200	m	99.00%	99.00%	
NEdT	baseline		97.00%	97.00%	
Calibration	baseline		99.00%	99.00%	
MTF	baseline		97.00%	97.00%	
band to band misregistration	0.2	pixels			

3.3.8 Numerical Computation Considerations

Bispectral cloud detection tests are computationally inexpensive. However, it is important that pixels are only detected as cloud a single time; therefore, the most efficient cloud detection test is applied first to all pixels. Those pixels classified as cloud-contaminated are removed, flagged, and the second cloud test is applied only to those remaining cloud-free, and so forth. Adjustments for special effects, e.g., partially cloudy pixels and shadows, are made only after all cloud tests have been applied and pixels identified as cloud-contaminated have been flagged.

3.3.9 Quality Assessment and Diagnostics

The accuracy of the cloud mask will be based upon the ground truth cloud mask as described in the Imagery ATBD [*V-1*](Topping *et al*., 1998).

3.3.10 Programming and Procedural Considerations

The VCM has been developed using FORTRAN77/90 on an SGI.

3.3.11 Quality Assessment and Diagnostics

The accuracy of the cloud mask will be based upon the ground truth cloud mask as described in the Imagery ATBD [V-1] (Topping *et al*., 1998).

3.4 VIIRS CLOUD MASK VALIDATION

The VCM algorithm validation presently underway, is based on the inter-comparison of clouds simulated using the Radiative Transfer code with the true cloud scenes being simulated.

Synthetic Imagery Data Sets

The synthetic imagery data sets used for Cloud Mask validation and verification were generated using the UCLA Radiative Transfer (RT) model, described in the VIIRS Cloud Optical Thickness and Effective Particle Size ATBD, and the TASC Cloud Scene Simulation Model (CSSM). The process used to generate synthetic scene is illustrated in Figure 15.

The UCLA RT model is executed over a wide range of effective particle sizes and optical depths, for specified atmospheric scenario, sensor geometry, solar geometry, VIIRS channels, and cloud type, altitude and thickness. The results are stored in the UCLA Radiance Look-up Tables (LUTs). The Radiance LUTs are used in conjunction with data from the TASC CSSM, which is described in more detail below, to create synthetic radiance images for the VIIRS bands. The Cloud EDR algorithms are applied to the synthetic imagery and retrievals are performed at the pixel-level. The pixel-level retrieval results are aggregated to the appropriate Horizontal Cell Size (HCS) for the EDR and compared with truth.

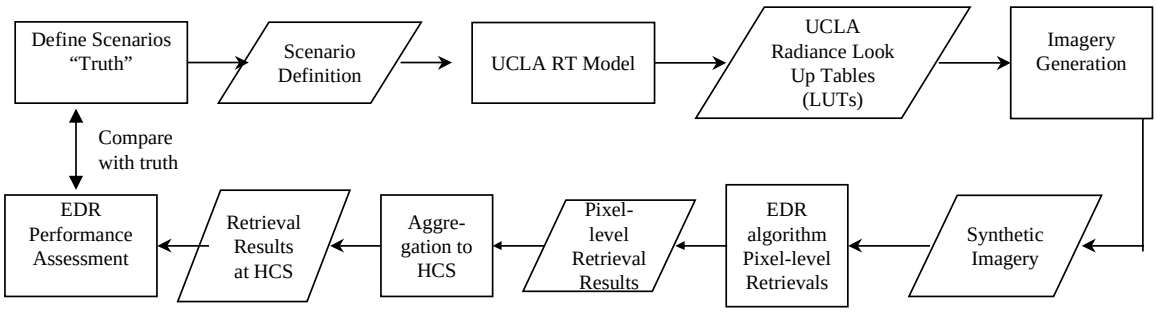

Figure 15. High level diagram of the synthetic imagery generation and performance assessment process for the Cloud EDRs.

Figure 16 focuses on the Imagery Generation box of Figure 15. CSSM is used to generate 3-D fields of cloud liquid water (CLW) or cloud ice water content (IWC) for specified cloud type, cloud coverage, etc. In the scene generation process for Cloud EDR Testing, CSSM is used to generate 3-D synthetic cirrus and water droplet cloud distributions over a 100x100 km area at 0.1 km spatial resolution throughout the volume. These data are vertically integrated to form grids of Ice Water Path (IWP) or Cloud Liquid Water (CLW), depending upon the cloud type, at 0.1 km resolution over the 100x100 km region. The IWP and CLW data are converted to visible optical depth using standard relationships for each cloud type (water or ice). In addition, a scaling factor is used to tune the resultant optical depth grids, such that all values fall within a specified range, e.g to support stratification tests. The optical depth grids are used in conjunction with the Radiance LUTs to create 100 x 100 km radiance images at 0.1 km resolution for each VIIRS cloud channel. Within each image, cloud top height, cloud thickness, and cloud effective particle size are set to nominal values over the entire image, consistent with the radiance data. Cloud optical thickness, however, varies considerably over the image. At this stage of the processing, sensor characteristics such as MTF, band-to-band miss-registration, calibration, and geolocation errors are introduced, as necessary. The 0.1 km radiances are aggregated to the appropriate VIIRS pixel size, which varies according to sensor viewing geometry. Pixel-level sensor noise is the introduced, resulting in synthetic imagery which include sensor effects.

Because VIIRS pixel level radiances are generated from higher resolution data, the resultant simulated VIIRS imagery contains cloud edge effects (mixture of clear and cloud radiances) and variation of optical depth even within the pixel. This has resulted in a very challenging retrieval environment to test the Cloud Mask algorithm.

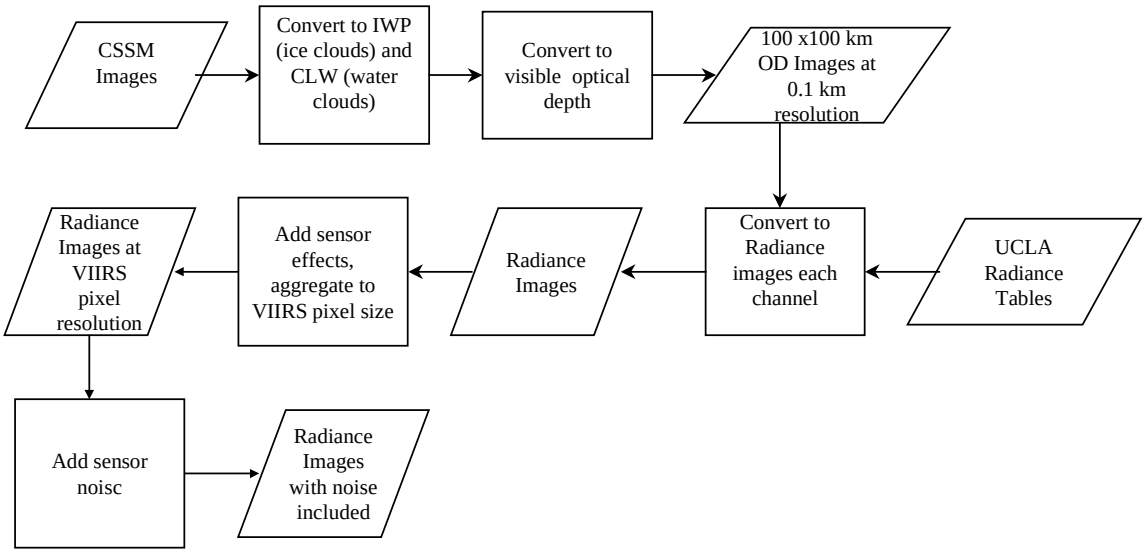

Figure 16. Imagery generation process using CSSM data, Radiance LUTs, and Sensor data.

For the simulated scenes discussed above, TASC generated cloudy scenes for varying cloud optical properties, height, phase, atmospheric type, and underlying surfaces. The number of possible scenes which might be used for cloud mask validation is overwhelming to consider. Therefore only a limited number of scenes will be demonstrated for each retrieval. The scenes considered are illustrated in Table 9. The band reflectances for the various surface types considered in these examples are shown in Table 7.

A number of analyses have been, and are currently being, performed in order to evaluate the performance of the algorithm under a variety of scenarios. Many of the sections that follow are a work in progress and will be substantially modified and expanded upon in the future. Table 9 summarizes the limited list of scenarios presently being used for simulation. This list of scenarios will greatly increase in the future.

Table 9. Scenario List of Simulated Data used for the VCM

Scenarios	Description	Surface Type
Scene #1	Ice Cloud (9-10 km), Midlatitude, Nadir, Solar Z = 32	Vegetative
Scene #2	Ice Cloud (9-10 km), Midlatitude, Nadir, Night	Vegetative
Scene #3	Water Cloud (1-2 km), Midlatitude, Nadir, Solar Z = 32	Vegetative
Scene #4	Water Cloud (1-2 km), Midlatitude, Nadir, Night	Vegetative
Scene #26	Ice cloud (9-10 km), Midlatitude, Nadir, Solar Z = 32	Ocean
Scene #27	Ice Cloud (9-10 km), Midlatitude, Nadir, Night	Ocean
Scene #28	Water Cloud (1-2 km), Midlatitude, Nadir, Solar Z = 32	Ocean
Scene #29	Water Cloud (1-2 km), Midlatitude, Nadir, Night	Ocean

Initial testing of the VCM was for a few scenes.

3.4.1 Retrieval Example Over Vegetated Land

As is shown in Table 8, two different cloud types were considered over vegetated land.

3.4.1.1 Water Cloud Over Vegetated Land

The first retrieval example will be the water cloud over vegetated land. The reflectances for the solar bands, and BT's for the thermal bands, are shown in Figures 17a-e.

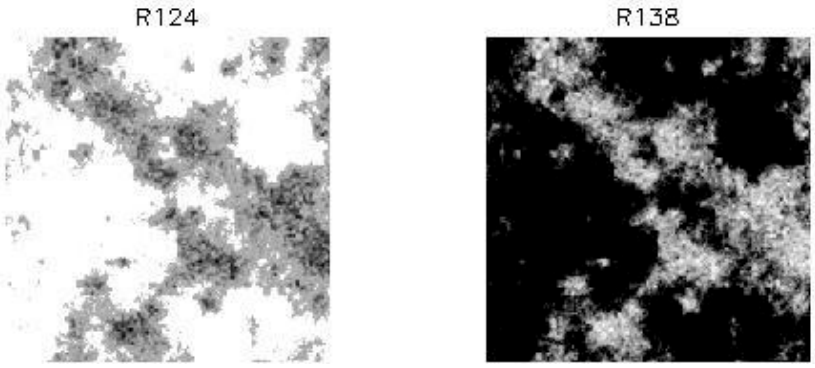

Figure 17a. Reflectance for water cloud scene at 0.65 and 0.86 microns.

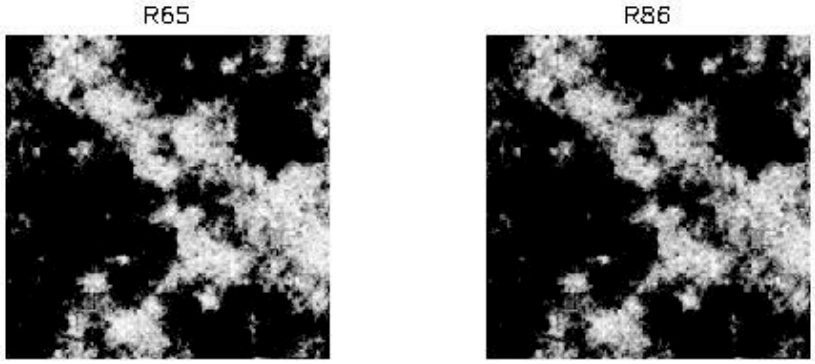

Figure 17b. Reflectance for water cloud scene at 1.24 and 1.38 microns.

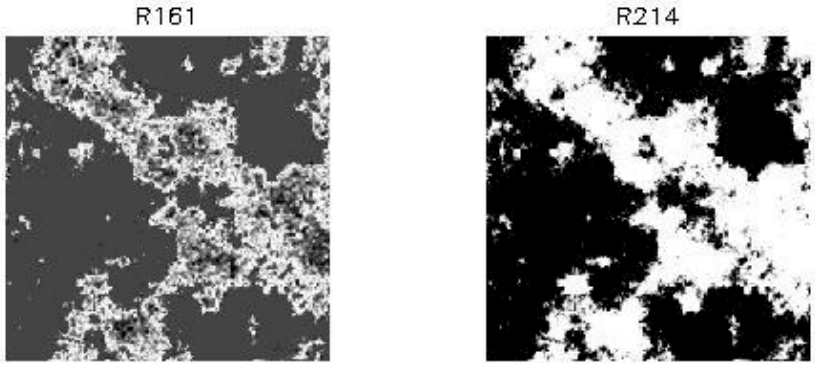

Figure 17c. Reflectance for water cloud scene at 1.61 and 2.14 microns.

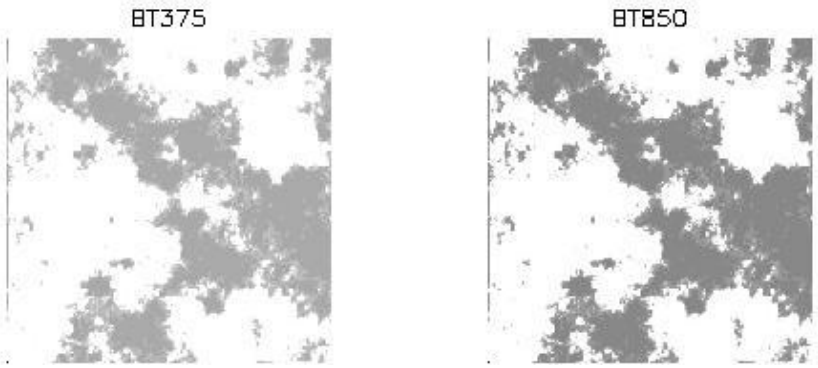

Figure 17d. BT for water cloud scene at 3.75 and 8.5 microns.

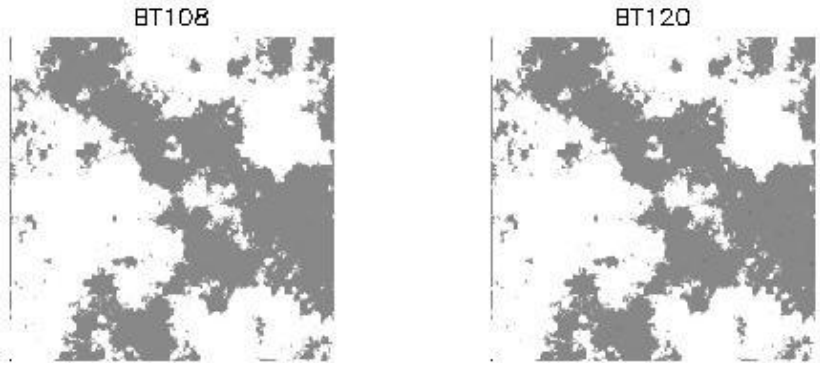

Figure 17e. BT for water cloud scene at 10.8 and 12.0 microns.

In Figures 17a-e above, the amount of information in the scene is displayed. Over different spectral bands, the underlying surface reflectance varies from that of the water clouds. In the BT images, the underlying surface is predominantly warmer than the water clouds in the scene. Using tests discussed in Section 3.3, the VCM generates cloud mask results, which are displayed in Figure 6. In this figure, the cloud mask is shown in gray, while black represents a negative cloud detection result. The three images in Figure 18 display the cloud mask for three cases. The image on the left displays what is referred to as "Tau-Truth." This represents cases where the optical thickness of the cloud displayed is greater than 0.03 at 0.65 microns. This definition of a cloud comes directly from the definitions section of the VIIRS Sensor Requirements Document (SRD). The middle image is of the cloud mask results in the daytime. The far right image is the cloud mask results at night.

The image shows that the cloud mask performance is very good for this scene. Note that this case (water clouds over land) is considered, due to the reflective and BT properties of land versus clouds, to be one of the easier cases that will be encountered by the VCM.

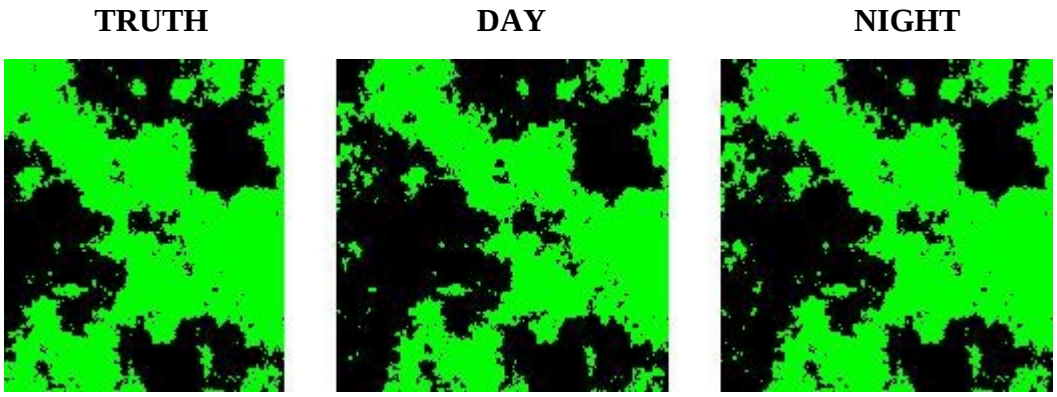

Figure 18. VCM results for water cloud scene for 'Tau-Truth', day, and night cases.

3.4.1.2 Cirrus Cloud Over Vegetated Land

This next retrieval example will be for a thin cirrus cloud over vegetated land. The reflectances for the solar bands and BTs for the thermal bands are shown in Figures 19a-e. The cloud mask results are displayed in Figure 20.

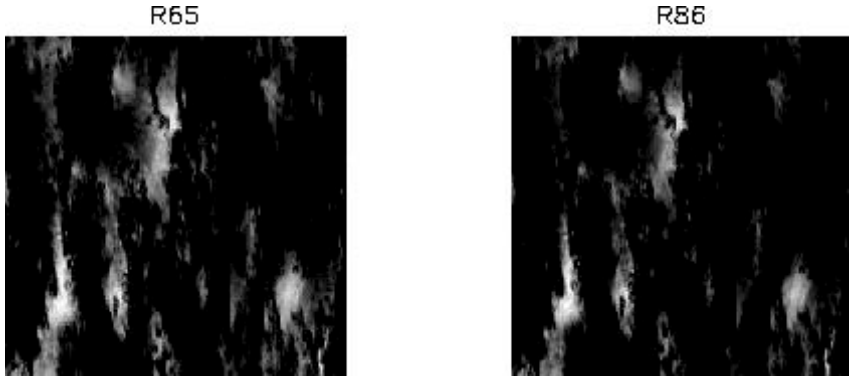

Figure 19a. Reflectances for cirrus cloud scene at 0.65 and 0.86 microns.

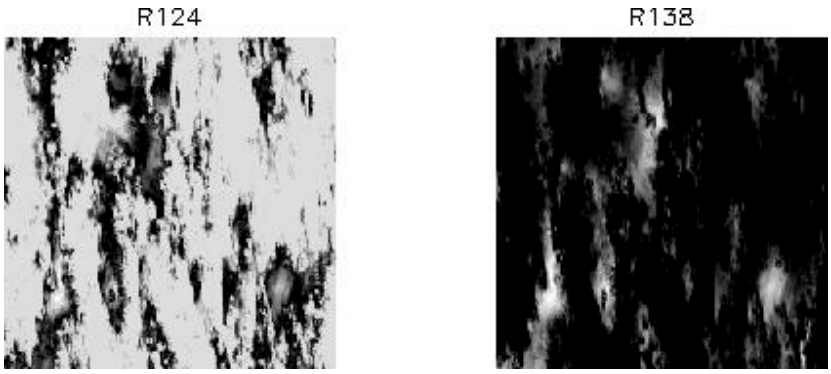

Figure 19b. Reflectances for cirrus cloud scene at 1.24 and 1.38 microns.

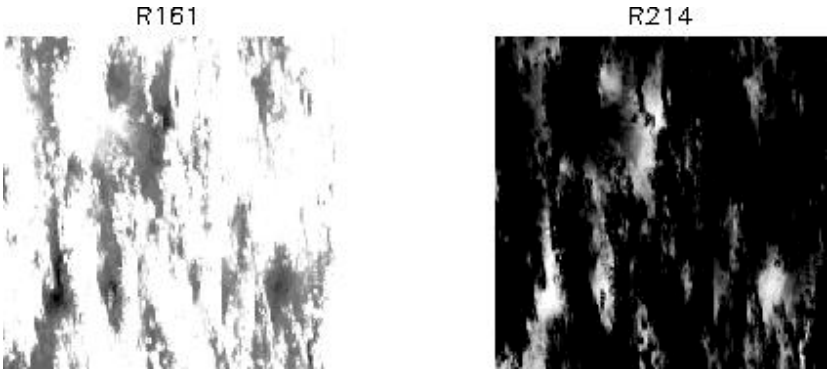

Figure 19c. Reflectances for cirrus cloud scene at 1.61 and 2.14 microns.

Figure 19d. BTs for cirrus cloud scene at 3.75 and 8.5 microns.

Figure 19e. BTs for cirrus cloud scene at 10.8 and 12.0 microns.

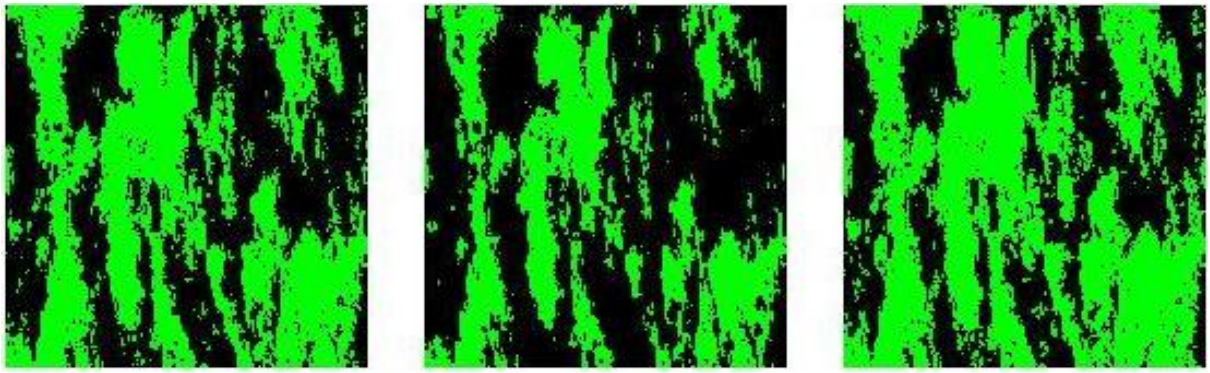

TRUTH DAY NIGHT

Figure 20. VCM Cloud Mask results for cirrus cloud 'Tau-Truth', day, and night cases.

The VCM is also being tested and validated over MAS data. Figure 21 is an example of the VCM applied over a MAS image, taken during the ARMCAS campaign of June 1995, in which a large cumulonimbus cloud has formed. In this image on the right is the RGB (Red-Green-Blue) image of the 2.14, 1.60, and the 0.65 micron bands are applied to demonstrate the multispectral capabilities of the VIIRS bands. The MAS bands are spectrally quite similar to the analogous VIIRS bands. The image on the left demonstrates the present VCM being applied over a MAS image..

3.4.2 Example Retrieval Over Snow/Ice

Development of the VCM over snow/ice surfaces has been done. The VCM is has been applied over sea/ice MAS data to develop its masking capabilities. Figure 22 is an example of an application of the VCM over the sea ice in the Bering Sea from the MAS ARMCAS campaign. The figure to the left is an RGB, Red = 1.88 microns, Green=1.6 microns, Blue= 0.55 microns, demonstrates the multi-spectral capabilities of the VCM, in which the 1.88 micron band is analogous in behavior to the 1.38 micron band of the VCM and the 0.55 micron band is analogous to the .65 micron band. In the image you can see the stratus deck quite clearly and the thin cirrus is bright in the 1.88 micron band, depicted as red in this RGB. The image to the right in this figure depicts the VCM results applied over this scene. It is noteworthy the capability that the cloud mask has of detecting thin cirrus clouds, near the bottom of the scene.

3.4.3 Predicted Performances of the VCM

The Probability of Correct Typing of the Cloud Mask are shown if Table 10. These values are based upon the assessed performances of the MCM, which the VCM will do at least as good as, and performance may exceed that of the MCM, and upon the CSSM and UCLA Radiative Transfer code simulated scenes used in VCM development. The performance assessment of the MCM was performed by a cloud imagery analyst at Raytheon, and the MCM performances are shown in Table 10.

The Probability of Correct Typing performance was of the MCM and thus the VCM was assessed by considering MAS scenes with ice and water clouds, of varying optical thickness. Optical thickness was known for the simulated data and for MAS scenes was assessed by the analyst. Probability of the VCM is in general 99.99% for very optically thick clouds, greater

than 10 optical thickness. While the lowest Probability of Correct Typing are for optically thin clouds at night, being approximately 82%. Looking at table 10 one can state that the performance for the Cloud Mask for optically thick clouds, greater than 5 optical depth, is greater than 99%, while for thin clouds, less than .5 optical depth, the performance range is between 82 and 89%. In general the performance of the Cloud Mask increases towards Edge of Scan (EOS), and is better at day than at night due to the wealth of spectral information available during the day vs. night. Also, over snow/ice and desert surfaces the cloud detection is less than over water and land surfaces.

The greatest increases in performances and largest changes in the probability of correct typing are expected to occur in the optically thin cloud cases and over the desert and snow/ice surface types. It is expected that these values will improve with the proper setting of the cloud detection thresholds and with the additional tests being performed by the VCM beyond those which the MCM does. Subpixel cloud detection using the Imagery bands will also assist greatly in the detection of clouds, and increase the performance.

Table 10a. Probability of Correct Typing of the VCM (Based upon MCM performance and simulated radiances using UCLA and CMMS)

Day				Probability of Correct Typing			
Cloud Type	Optical Depth	Nadir	EOS	Vegetated Land	Water	Desert	Snow/Ice
Water	0.03 - 0.5	x		87.00	92.00	87.00	88.00
Water	0.03 - 0.5		x	88.00	92.00	88.00	89.00
Water	0.5 - 1.0	x		99.90	98.90	97.00	95.00
Water	0.5 - 1.0		x	99.90	99.10	98.85	96.00
Water	1.0 - 10.0	x		99.96	99.99	98.90	96.00
Water	1.0 - 10.0		x	99.97	99.99	99.50	96.00
Water	> 10.0	x		99.99	99.99	99.99	99.50
Water	> 10.0		x	99.99	99.99	99.99	99.50
Ice	0.03 - 0.1	x		88.00	92.00	90.00	85.00
Ice	0.03 - 0.1		x	89.00	95.00	92.00	88.00
Ice	0.1 - 1.0	x		99.20	97.50	95.00	93.00
Ice	0.1 - 1.0		x	99.25	98.50	96.00	94.50
Ice	1.0 - 10.0	x		99.90	99.94	97.50	95.00
Ice	1.0 - 10.0		x	99.90	99.96	98.50	95.50
Ice	> 10.0	x		99.99	99.99	98.40	96.00
Ice	> 10.0		x	99.99	99.99	98.50	96.50

Table 10b. Probability of Correct Typing of the VCM (Based upon MCM performance and simulated radiances using UCLA and CMMS)

Night				Probability of Correct Typing			
Cloud Type	Optical Depth	Nadir	EOS	Vegetated Land	Water	Desert	Snow/Ice
Water	0.03 - 0.5	x		87.00	90.00	86.00	85.00
Water	0.03 - 0.5		x	88.00	91.00	87.00	86.00
Water	0.5 - 1.0	x		97.50	96.50	94.00	90.00
Water	0.5 - 1.0		x	98.00	97.50	95.00	91.00
Water	1.0 - 5.0	x		98.50	99.50	96.50	92.00
Water	1.0 - 5.0		x	98.75	99.50	97.00	93.50
Water	5.0 - 10.0	x		99.99	99.99	97.50	96.00
Water	5.0 - 10.0		x	99.99	99.99	98.00	97.00
Water	> 10.0	x		99.99	99.99	98.50	98.50
Water	> 10.0		x	99.99	99.99	99.00	99.50
Ice	0.03 - 0.1	x		87.00	90.00	86.00	85.00
Ice	0.03 - 0.1		x	88.00	91.00	87.00	86.00
Ice	0.1 - 1.0	x		93.00	94.00	89.00	87.00
Ice	0.1 - 1.0		x	94.00	95.00	90.00	88.00
Ice	1.0 - 5.0	x		96.00	96.00	94.00	90.00
Ice	1.0 - 5.0		x	96.50	97.50	95.00	91.00
Ice	5.0 - 10.0	x		98.00	98.00	96.00	96.00
Ice	5.0 - 10.0		x	98.50	98.50	97.00	97.00
Ice	> 10.0	x		99.99	99.99	99.00	99.00
Ice	> 10.0		x	99.99	99.99	99.50	99.50

VIIRS Cloud Mask Over Land

RGB **Cloud Mask Overlayed on 0.65 µm**

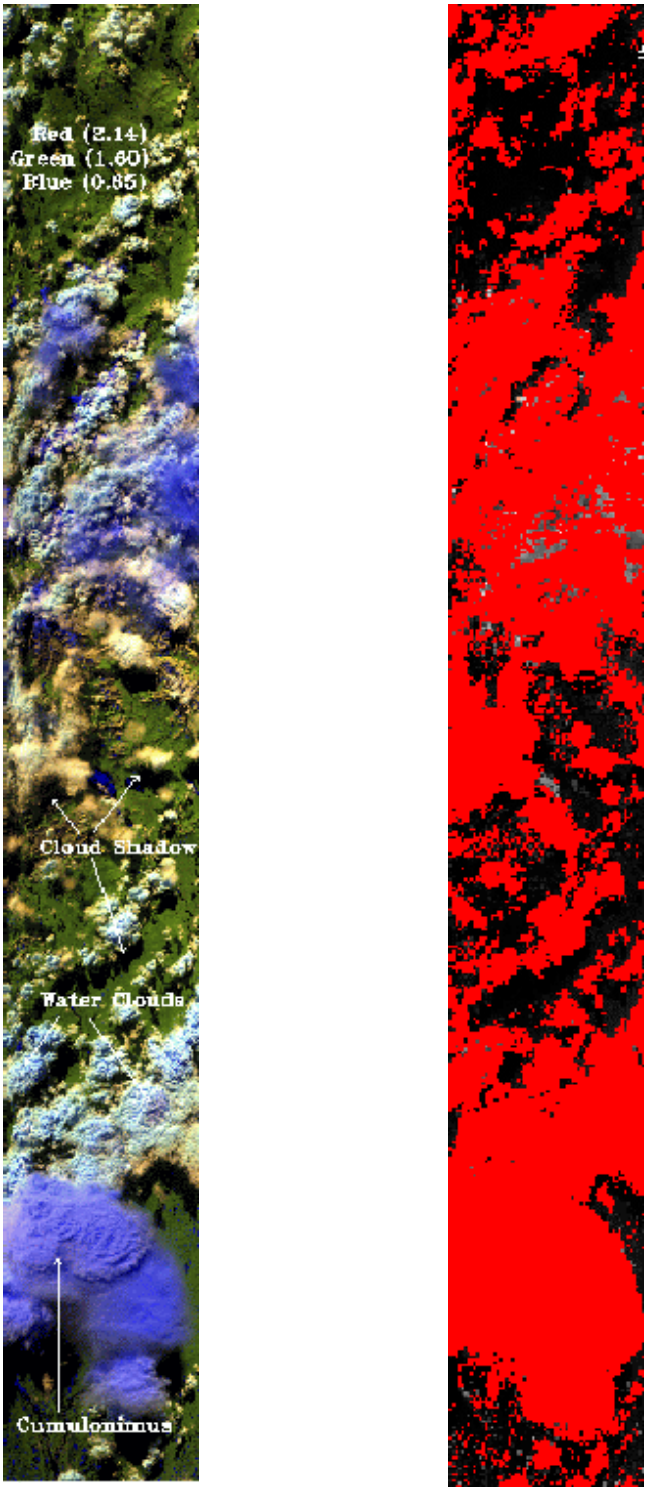

Figure 21. VCM applied over land during the MAS ARMCAS Campaign.

VIIRS Cloud Mask Over Sea Ice

RGB

Cloud Mask Overlayed on 0.65 μm

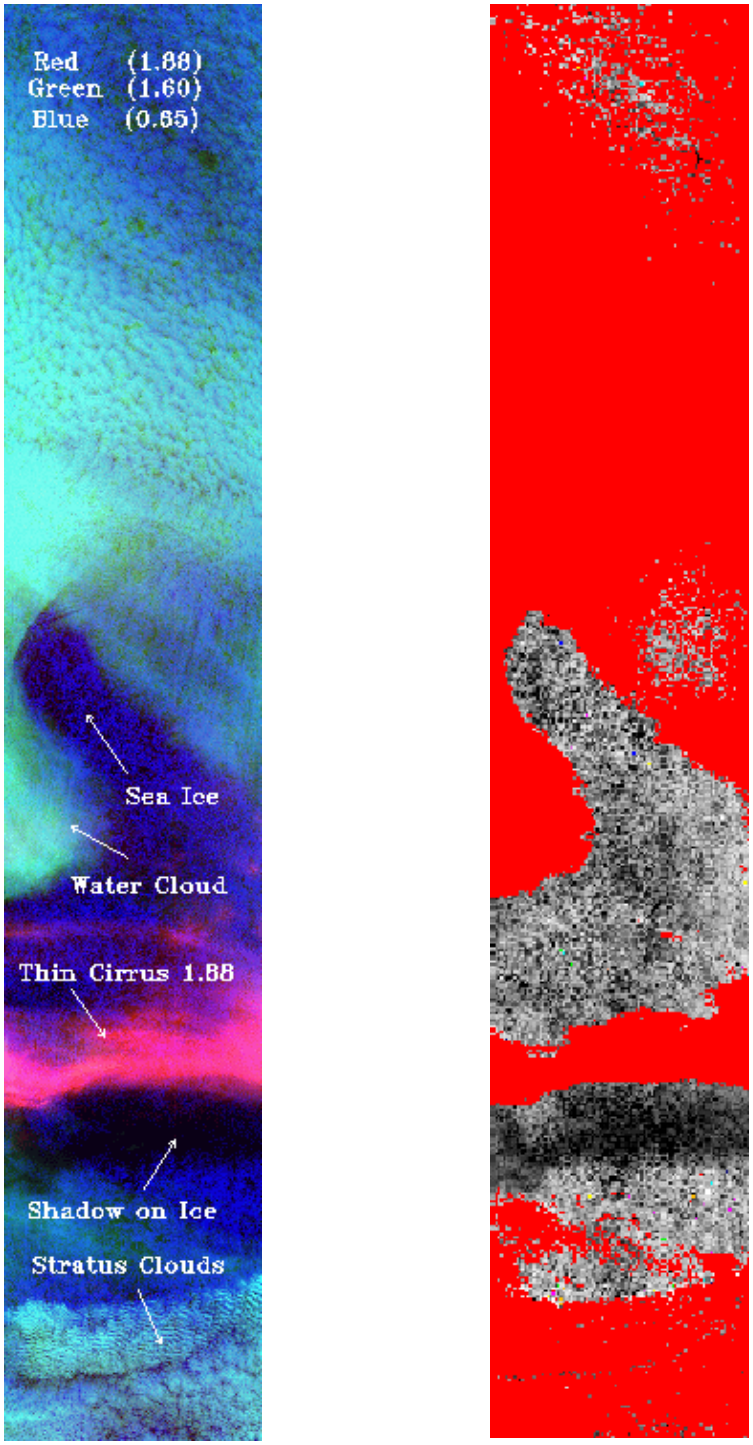

Figure 22. VCM over sea ice during the MAS ARMCAS campaign.

3.5 VCM VALIDATION PLAN

The VIIRS Cloud Mask must perform well enough to meet or exceed the thresholds given by the IPO for the cloud mask-dependent EDRs. In order to evaluate the performance of the Cloud Mask and other Cloud EDR retrievals, the Cloud Validation Plan (CVP) is in the developmental stages. For any Cloud EDR, we define:

Algorithm validation constitutes a comparison between:

- geophysical products retrieved by applying VIIRS-EDR algorithms to surface or tropospheric-leaving radiances measured by a VIIRS simulator instrument or top-of-atmosphere (TOA) radiances measured by VIIRS.
- geophysical products retrieved from downwelling sky and solar radiation measured at the surface together with conventional retrieval algorithms based on such measurements. Analysis of systematic and random errors in each pathway (e.g., downward looking and upward looking) is included.

A *field experiment* is a comparison of two geophysical parameter retrievals based on independent measurements.

A *field campaign* is an activity which involves conducting one or more field experiments.

The CVP describes how, in the pre-launch period, an output is generated which accurately represents (in a scientific sense) what it purports to. Secondly, the plan describes how each data product, in the post-launch period, can be shown to accurately represent the corresponding radiometric or environmental ("geophysical") parameters. The plan contains the following elements:

- Description of validation objectives
- Specification of VIIRS products that can be validated by simple ground-based or aircraft based procedures
- Specification of conventional methods for measuring each product from ground perspective
- Definition of algorithm development needs, beyond that existing and available
- Definition of instrumentation needs, uses, calibration, and intercomparison procedures, including:
  - ground-based for applicable atmosphere, surface, and TOA/cloud retrievals;
  - aircraft VIIRS simulator and supporting instruments (e.g., aircraft sunphotometry) and aircraft measurements (e.g., *in situ* cloud sampling);
  - spacecraft candidates with view capabilities that bear upon comparisons with VIIRS;
  - Specification of test sites for both algorithm validation (pre-launch) and product verification (post-launch);
  - Description of the nature of field experiments to achieve simultaneous ground-based and aircraft simulator (pre-launch) or VIIRS (post-launch) observations, including required

experimental conditions, deployment of ground-based resources, aircraft flight line configurations, and timing of overpasses to simulate VIIRS observing conditions;

- Description of post-experiment data reduction and error analysis procedures; and
- Plans for archival and publication of validation/verification results.

The CVP is designed to accomplish the following objectives in the pre-launch and post-launch time frames.

3.5.1 Pre-Launch

- Validate the Cloud EDRs using simulated data
- Procurement and adaptation/modification of essential field instruments for solar, cloudy, clear sky and ground-reflected radiation measurements to implement cloud retrieval algorithms
- Organization of field campaigns at selected test sites, encompassing essential parts of the different surface and cloudy conditions on a global scale
- Demonstrate the ability to make field measurements of radiometric quantities
- Demonstrate the ability to derive the Cloud EDRs from ground measurements
- Specific evaluation of the sensitivity of VIIRS airborne simulator and field instruments to validate VIIRS EDR retrieval algorithms
- Develop new software to analyze data for VIIRS needs (e.g., software for CIMMEL or any other ground based instrument measured data)
- Cooperate and discuss with the calibration team the results of the measurements, simulations, and calibrations found for the VIIRS simulator instruments as well as the VIIRS sensor.

3.5.2 Post-Launch

- Validate the Cloud EDRs using satellite-derived data
- Continue to validate the Cloud EDRs as needed
- Discuss the measurements delivered by the VIIRS sensor with the calibration team
- Calibrate the VIIRS simulator instruments in constant time intervals to uncover instrument degradation and to keep track of possible changes in performance of the VIIRS sensor
- Conduct field experiments on the designated test-sites coordinated with *in situ* flights of airborne instruments and a VIIRS overpass
- Comparison/analysis of VIIRS derived cloud EDRs and analogous EDRs derived from other satellite systems.

For the intercomparison of ground/airborne and satellite-derived data, different instruments are listed in Tables 11 through 13. These instruments are presently deployed by NSF, DOE, and NOAA sites, and have been deployed in various NASA, DOE, NSF, and NOAA campaigns in the past.

Table 11. Ground based instruments for the CVP.

Ground Measurements	
Instrument	**Purpose**
NIP	Cloud cover validation
PSP	Cloud cover validation
MFRSR	Cloud optical thickness validation
IRT	Cloud cover validation
CSPOT	Cloud optical thickness validation
AERI	Cloud cover validation
WSI	Cloud cover validation
BLC	Cloud Base Validation
GUV	Cloud Effective Optical Thickness validation
GPS	Geolocation
BLC	Cloud Base Height validation
WSI	Whole Sky imaging; cloud cover observations
VTLC	Cloud validation
VCEIL	Multi-layered cloud validation
RL	Cloud validation, multi-layer cloud detection
MWR	Cloud phase determination
MMCR	Cloud boundary determination, top and base
MPL	Cloud Validation, multi-layer cloud detection
RSS	Cloud cover and optical thickness validation
SMOS	Surface Measurements, snow validation
SMET	Meteorology, cloud cover observations

3.5.3 Explanation of Ground Based Instruments

Belfort Laser Ceilometer (BLC).

The Model 7013C Ceilometer field unit is a self-contained, ground-based, optical, active remote sensing instrument with the ability to detect and process several cloud-related parameters. These parameters include cloud height, extinction coefficient, cloud layers and time/date reference information. The ceilometer system detects clouds by transmitting pulses of infrared light vertically into the atmosphere. The receiver telescope detects scattered light from clouds and precipitation.

Table 12. Airborne instruments for the CVP.

Airborne Measurements	
Instrument	**Purpose**
BBSS	Balloon borne sounding system, atmospheric profiles
ER-2	Platform for instruments
AVIRIS	Nadir viewing multi-spectral images
UW CV-580 (U. Washington)	Met., aerosol/cloud properties, radiometry
NCAR C-130	Met., aerosol/cloud properties, radiometry
Camera (e.g., Nikon, FOV: 180°)	Cloud detection, imagery
CLS	Cloud Lidar System, cloud detection
CAR	Multi-angle spectral images, cloud absorption properties
GPS	Geolocation
MAS	MODIS Airborne Simulator
RC-10	Aerial photographs

Table 13. Satellite to compare with VIIRS for the CVP.

Satellite Measurements	
Instrument	**Purpose**
MISR	
MERIS	
AMSR	
GLI	Intercomparison with VIIRS Cloud EDRs
Landsat	Intercomparison with VIIRS Cloud EDRs
AVHRR	Intercomparison with VIIRS Cloud EDRs
MODIS	Intercomparison with VIIRS Cloud EDRs

Micropulse Lidar (MPL). The Micropulse Lidar (MPL) is a ground-based optical remote sensing system designed primarily to determine the altitude of clouds overhead. The physical principle is the same as for radar. A pulse of energy is transmitted and the energy that is reflected back is measured. From the time delay between the transmitted pulse and the backscattered signal, the distance to the scatterer is inferred. Besides real-time detection of clouds, post-processing can also characterize the extent of the tropospheric mixing layer (the planetary boundary layer), or other particle-laden regions. This eye-safe system is designed for continuous operation.

Millimeter Wave Cloud Radar (MMCR). The MMCR is a zenith-pointing radar that operates at a frequency of 35 GHz. The main purpose of this radar is to determine cloud boundaries (e.g., cloud bottoms and tops). This radar will also report radar reflectivity (dBZ) of the atmosphere up to 20 km. The radar possesses a doppler capability that will allow the measurement of cloud constituent vertical velocities.

Microwave Water Radiometer (MWR). The Microwave Water Radiometer (MWR) provides time-series measurements of column-integrated amounts of water vapor and liquid water. The instrument itself is essentially a sensitive microwave receiver. That is, it is tuned to measure the microwave emissions of the vapor and liquid water molecules in the atmosphere at specific frequencies.

CART Raman Lidar (RL). The CART Raman Lidar (RL) is an active, ground-based laser remote sensing instrument that measures vertical profiles of water-vapor mixing ratio and several cloud- and aerosol-related quantities. Lidar (light detection and ranging) is the optical analog of radar, using pulses of laser radiation to probe the atmosphere. This system is fully computer automated, and may run unattended for many days following a brief (~5-minute) startup period. The self-contained system (requiring only external electrical power) is housed in a climate-controlled 8'x8'x20' standard shipping container.

Vaisala Ceilometer (Model CT25K). The Vaisala Ceilometer (VCEIL) is a self-contained, ground-based, active, remote sensing device designed to measure cloud base height at up to three levels and potentially backscatter signals by aerosols. Model CT25K has a maximum vertical range of 25,000. The ceilometer transmits near-infrared pulses of light and the receiver telescope detects the light scattered back by clouds and precipitation.

Video Time-Lapsed Camera (VTLC). The Video Time-Lapsed Camera provides a record of sky conditions by recording color images of an approximately 100-degree field of view, centered on the zenith. The time interval between images may be adjusted to a wide range of periods, but typically is set to 4 or 8 seconds, thus providing a high time resolution record of cloud conditions. Data is stored to S-VHS tape for archival.

Whole-Sky Imager (WSI). The Whole-Sky Imager (WSI) is an automated imager used for assessing and documenting cloud fields and cloud field dynamics. The WSI is a ground-based electronic imaging system that monitors the upper hemisphere. It is a passive, i.e., non-emissive, system that acquires images of the sky dome through three spectral filters (neutral, red, and blue). From these sky images, we can assess the presence, distribution, shape, and radiance of clouds over the entire sky using automated cloud decision algorithms and related processing. The current WSI model (EOSystem6) is capable of image acquisition under daylight, moonlight, and starlight conditions.

Atmospheric Emitted Radiance Interferometer (AERI). The Atmospheric Emitted Radiance Interferometer (AERI) measures the absolute infrared spectral radiance (watts per square meter per steradian per wavenumber) of the sky directly above the instrument. The spectral measurement range of the instrument is 500 to 3300 wavenumbers(cm-1) or 20 to 3 microns. Spectral resolution is 1.0 cm-1. Instrument field-of-view is 1.3 degrees. A calibrated sky radiance spectrum is produced every 10 minutes. The AERI data can be used for: 1) evaluation

of line-by-line radiative transport codes; 2) detection/ quantification of cloud effects on ground-based measurements of infrared spectral radiance and; 3) calculation of vertical atmospheric profiles of temperature and water vapor.

Cimel Sunphotometer (CSPOT). The CSPOT is a multi-channel, automatic sun- and sky-scanning radiometer that measures the direct solar irradiance and sky radiance at the earth's surface. Measurements are taken at predetermined discrete wavelengths in the visible and near-IR parts of the spectrum to determine atmospheric transmission and scattering properties. This instrument is weather-proof and requires little maintenance during periods of adverse weather conditions. It takes measurements only during daylight hours (sun above horizon).

Infrared Thermometer (IRT). The Infrared Thermometer (IRT) is a ground-based radiation pyrometer that provides measurements of the equivalent black body brightness temperature of the scene in its field of view. The up-looking version has a narrow field of view for measuring sky temperature and for detecting clouds. The down-looking version has a wide field of view for measuring the narrowband radiating temperature of the ground surface.T).

Multi-Filter Rotating Shadowband Radiometer (MFRSR). The MFRSR takes spectral measurements of direct normal, diffuse horizontal, and total horizontal solar irradiances. These measurements are at nominal wavelengths of 415, 500, 610, 665, 862 and 940 nm. The measurements are made at a user specified time interval; typically this interval is about one minute or less. (the sampling interval is 20 seconds.) From such measurements, one may infer the atmosphere's optical depth at the wavelengths mentioned above. In turn, these optical depths may be used to derive information about the column abundances of ozone and water vapor, as well as aerosol and other atmospheric constituents. A silicon detector is also part of the MFRSR. This broadband detector provides a measure of the broadband direct normal, diffuse horizontal, and total horizontal solar irradiances. These quantities are uncalibrated and reported in units of "counts."

SKYRAD Shaded Precision Spectral Pyranometer (PSP). The PSP measures the amount of solar radiation (sunshine) that falls on the sensor under a clear dome. When the PSP is mounted on the solar tracker and shaded from the direct beam of the sun it measures only that part of the solar radiation that is scattered downward by clouds, other material in the air, and the air itself. The value is called the “diffuse” solar irradiance. On a clear day around noon it should measure about 100 watts per square meter. The diffuse component will increase when clouds are present.

Normal Incidence Pyrheliometer (NIP). The NIP is like a narrow view telescope. It has a sensor at the viewing end that measures the amount of solar radiation that falls on it. The NIP is mounted on the solar tracker so that it is always pointing directly at the sun. The value that it measures is called the “direct” solar irradiance and on a clear day at noon it will have a value of about 1000 watts per square meter. This value will decrease when the sun is lower in the sky. When thick clouds are present (that is, when the solar disk cannot be seen), the NIP should measure approximately zero.

Rotating Shadowband Spectrometer (RSS). The Rotating Shadowband Spectroradiometer (RSS) provides spectral direct, diffuse, and total horizontal irradiances over the wavelength range from 350 to 1075 nm. This portion of the shortwave spectrum represents about 75 percent

of the total energy from the sun. The RSS implements the same automated shadowbanding technique used by the MFRSR, and so it too provides spectrally-resolved direct-normal, diffuse-horizontal, and total-horizontal irradiances, and can be calibrated *in situ* via Langley regression.

Surface Meteorology (SMET). The Surface Meteorology station (SMET) uses mainly conventional *in situ* sensors to obtain 1-minute statistics of surface wind speed, wind direction, air temperature, relative humidity, barometric pressure, and rain-rate.

Surface Meteorological Observation System (SMOS). The Surface Meteorological Observation System (SMOS) mostly uses conventional *in situ* sensors to obtain one-minute and thirty-minute averages of surface wind speed, wind direction, air temperature, relative humidity, barometric pressure, and precipitation. A measure of local snow depth is also made at each SMOS with an ultrasonic device.

Ground Based Ultraviolet (GUV). The Biospherical Instruments Ground-based Ultraviolet GTR-511 Radiometer is designed to monitor UV radiation as it impacts our environment--providing key UV wavelength data for biological exposure studies. These wavelengths allow the extraction of cloud optical thickness and total column ozone, two critical variables used in modeling the solar spectrum. The systems are designed to be easily deployed, either individually or in networks, to examine the geographic variability in UV exposure.

ER-2 Aircraft Program. The ER-2 is a civilian version of the U.S. Air Force U2-S reconnaissance platform. These high-altitude aircraft are used as platforms for investigations that cannot be accomplished by sensor platforms of the private sector. Aircraft and spacecraft have proven to be excellent platforms for remote and *in situ* sensing. The ER-2, flying at the edge of space, can scan shorelines, measure water levels, help fight forest fires, profile the atmosphere, assess flood damage, and sample the stratosphere.

Balloon-Borne Sounding System (BBSS). The Balloon-Borne Sounding System (BBSS) provides *in situ* measurements (vertical profiles) of both the thermodynamic state of the atmosphere and the wind speed and direction. These are deployed at ARM sites around the world.

Cloud Absorption Radiometer (CAR). This instrument is a multi-wavelength scanning radiometer that measures the angular distribution of scattered radiation. Originally designed to determine the single scattering albedo of clouds at selected wavelengths in the visible and near-infrared, the CAR has been applied to scientific problems that have evolved dramatically over the years. Nowadays, the CAR can also be used to measure bidirectional reflectance for various surface types or simply as an imaging system. Between 1985 and 1998, it had flown in the nose cone of the Convair C-131A aircraft operated by the University of Washington, Department of Atmospheric Sciences, in concert with an array of cloud microphysics, aerosol, atmospheric chemistry, and general meteorological instruments. CAR has been deployed on a regular basis on experiment campaigns around the world. These have included deployments to the Azores, Brazil, Kuwait, continental U.S. and Alaska. Since April 1998, the CAR instrument has been flown in the new nose cone of the University of Washington's Convair CV-580 aircraft.

MODIS Airborne Simulator (MAS). The MODIS Airborne Simulator (MAS) is modified Daedalus multispectral scanner. This airborne scanning spectrometer acquires high spatial resolution imagery of cloud and surface features from its vantage point onboard a NASA ER-2 high-altitude research aircraft. Measurements are taken at 50 narrowband channels between 0.44 and 14.2 microns. From a nominal ER-2 altitude of 20 km, images have a resolution of 50 meters at nadir. Data acquired by the MAS are helping to define, develop, and test algorithms for the Moderate Resolution Imaging Spectroradiometer (MODIS), a key sensor of NASA's Earth Observing System (EOS). The MODIS program will emphasize the use of remotely sensed data to monitor variation in environmental conditions for assessing both natural and human-induced global change.

Airborne Visible Infrared Imaging Spectrometer (AVIRIS). This instrument is a unique optical sensor that delivers calibrated images of the upwelling spectral radiance in 224 contiguous spectral channels with wavelengths from 400 to 2500 nm. The resolution of this instrument is 20 meters at nadir. The instrument flies aboard a NASA ER-2 airplane (a U-2 plane modified for increased performance) at approximately 20 km above sea level, at about 730 km/hr. AVIRIS has flown all across the U.S., Canada and Europe.

RC-10. The Wild-Heerbrug RC-10 metric mapping camera can be loaded with high definition color infrared, natural color, and black and white imulsion film in a 9 x 9 inch film format. This camera is flown on the ER-2. At the ER-2 altitude of 20km use of this camera provides aerial coverage of 16 x 16 nautical miles and a spatial resolution of 6 meters at nadir.

CLS. The Cloud Lidar System is a nadir viewing, monostatic lidar that provides the true height of cloud boundaries and the density structure of less dense clouds. It uses the Nd:YAG laser, transmitting at 0.532 and 1.064 microns. A pulse per second firing rate is normally employed. This allows measurements to be taken at 20 meter horizontal intervals at the nominal ER-2 speed of 200 m/s. The highest attainable vertical sampling resolution with this lidar is 7.5 meters. This allows the construction of detailed cloud topography and vertical structure in the nadir direction.

UW Research Plane. The University of Washington’s Convair CV-580 is an aircraft with instrumentation for general meteorological, cloud physics, aerosol, and atmospheric chemistry and radiation measurements. The instrumentation suite on board this craft is substantial.

NCAR Research Plane. TBD.

The following sensors to compare to VIIRS for intercomparison with the CVP are from the ADEOS-II (Advanced Earth Observing Satellite -II) platform, to be launched in 2000.

Advanced Microwave Scanning Radiometer (AMSR). AMSR will observe various physical content concerning water by receiving feeble microwave to be naturally radiated from the Earth's surface and atmosphere (for example, water vapor content, precipitation, sea surface temperature, sea surface wind, sea ice), regardless of day and night, the presence of cloud. This sensor aims to collect global data for grasping mainly the circulation of water and energy.

Global Imager (GLI). GLI is an optical sensor observing the reflected solar radiation from the earth's surface including land, ocean and cloud and/or the infrared radiation with multi-channel for measuring the biological content, such as chlorophyll, organic substance, vegetation index,

and temperature, snow and ice, cloud distribution. These data will be used for grasping the global circulation of carbon and climate change.

Other satellite sensors will be filled in here.

3.5.4 VIIRS Test Beds

The following guidelines have been applied for the selection of the NPOESS-VIIRS Test beds:

- Co-locate algorithm and product validation experiments where possible with other major surface and/or atmospheric experiments to take advantage of resources and infrastructure present and make possible the sharing of scientific data.
- Logistic convenience for surface and aircraft observations to minimize field access problems as well as aircraft flight hour costs. Sites may be occupied on a repeated basis over a period of years. Sites in North America and continental United States plus adjacent ocean waters have thus been favored whenever possible, except where significant advantages may be obtained by joining forces with other groups elsewhere.
- Availability of records of seasonal conditions to optimize chances for specific cloud coverage, cloud types, effective particle sizes, cloud heights, and optical depths.

Some of the test beds listed in Table 13 no longer exist. However, they have been chosen carefully and fulfill the requirements listed above. For reasons of data heritage, one or several of these test beds could be selected.

Aerosol Robotic NETwork (AERONET). This is an optical ground based aerosol monitoring network and data archive supported by NASA's Earth Observing System and expanded by federation with many non-NASA institutions. The network hardware consists of identical automatic sun-sky scanning spectral radiometers owned by national agencies and universities. Data from this collaboration provides globally distributed near real time observations of aerosol spectral optical depths, aerosol size distributions, and precipitable water in diverse aerosol regimes. The data undergo preliminary processing (real time data), reprocessing (final calibration ~6 mo. after data collection), quality assurance, archiving and distribution from NASA's Goddard Space Flight Center master archive and several identical data bases maintained globally. The data provide algorithm validation of satellite aerosol retrievals and as well as characterization of aerosol properties that are unavailable from satellite sensors.

The rest of the campaigns will be filled in here. (TBD)

Cloud EDR Validation Plan Milestones (to be specified)

- Perform the tasks listed above in the ‘pre-launch’ time frame.
- Prepare the post-launch activities listed above.

3.6 ALGORITHM DEVELOPMENT SCHEDULE

A strategy for the algorithm development, as well as a listing of key development milestones, are summarized in an algorithm tracking table in [*V-2*].

Table 14. Possible test beds for the CVP.

Possible Test Beds for Validation	
Instrument	**Purpose**
AERONET	Aerosol Network (World)
ARM CART	Atmospheric Radiation Measurement, Cloud and Radiation Test Bed (Oklahoma, Alaska, South Pacific)
ALASKA	MAS campaign 1995 (Alaska)
ARMCAS	Arctic Radiation Measurement in Column Atmosphere-Surface (Alaska)
ACE II	Aerosol Characterization Experiment (North Atlantic Region)
BOREAS	Boreal Ecosystem-Atmosphere Study (Canada)
MAST	Monterrey Area Ship Track (Pacific Ocean)
IABP	International Arctic Buoy Program
SHEBA	Surface Heat Energy Balance (Arctic Ocean)
FIRE - ACE	First ISCPP Regional Experiment III
EOPACE	Electro-optic Propagation Assessment in Coastal Environment (South/Central Calif.)
HAPEX-Sahel, FIFE, TRACE-A, SAFARI, LBA	Atm. Parameters over land cover gradients
ISIS	NOAA Integrated Surface Irradiance Study (US)
SCAR-A	Sulfates Cloud and Radiation (Central US)
SUCCESS	Subsonic Aircraft Contrail and Cloud (Central US)
SCAR-B	Smoke, Clouds, and Radiation (Brazil)
WINCE	WINter Cloud Experiment (Great Lakes/Canada)
TARFOX	Tropospheric Aerosol Radiative Forcing Observational Experiment (Coastal Eastern US in summer)
White Sands/Railroad Playa	Instrument calibration

4.0 REFERENCES

Ackerman, S. A., W. L. Smith and H. E. Revercomb (1990). The 27-28 October 1986 FIRE IFO Cirrus Case Study: Spectral Properties of Cirrus Clouds in the 8-12 Micron Window. *Mon. Wea. Rev*., 118, 2377-2388.

Ackerman, S. A., K. Strabala, P. Menzel, R. Frey, C. Moeller, L. Gumley, B. Baum, C. Schaaf, and G. Riggs (1997). Discriminating Clear-Sky From Cloud With MODIS Algorithm Theoretical Basis Document (MOD35). Version 3.2

Berk, A., L. S. Bernstein, and D. C. Roberson (1989). MODTRAN: A Moderate Resolution Model for LOWTRAN7, Report AFGL-TR-89-0122 (Air Force Geophysics Laboratory), Hanscom, AFB, MA 01731.

Gao, B. C., A. F. H. Goetz, and W. J. Wiscombe (1993). Cirrus Cloud Detection From Airborne Spectrometer Data Using the 1.38 Micron Water Vapor Band, *Geophys. Res. Lett*., 20, 301-304.

Goodman, A. H., and A. Henderson-Sellers (1988). Cloud Detection Analysis: A Review of Recent Progress. *Atm. Res*., 21, 203.

Gustafson, G. B., R. G. Isaacs, R. P. d'Entremont, J. M. Sparrow, T. M. Hamill, C. Grasotti, D. W. Johnson, C. P. Sarkisian, D. C. Peduzzi, B. T. Pearson, V. D. Jakabhazy, J. S. Belfiore, and A. S. Lisa (1994). Support of Environmental Requirements for Cloud Analysis and Archive (SERCAA): algorithm descriptions, PL-TR-94-2114, Phillips Laboratory, AFMC, Hanscom AFB, MA.

Hall, D. K., G. A. Riggs, and V. V. Solomonson (1995). Development of Methods for Mapping Global Snow Cover Using Moderate Resolution Imaging Spectroradiometer Data. *Remote Sens. Env*., 54, 127-140.

Hall, D. K., G. A. Riggs, and V. V. Solomonson (1996). Algorithm Theoretical Basis Document (ATBD) for the MODIS Snow-, Lake Ice-, and Sea Ice-Mapping Algorithms. Version 3.0.

Hutchison, K. D., and K. Hardy (1995). Threshold functions for automated cloud analyses of global meteorological satellite imagery. *International Journal of Remote Sensing*, 16, 3665-3680.

Hutchison, K. D., and N. Choe (1996). Application of 1.38 μm imagery for thin cirrus detection in daytime imagery collected over land surfaces. *International Journal of Remote Sensing*, 17, 3325-3342.

Hutchison, K. D., and J. K. Locke (1997). Snow Identification through Cirrus Cloudy Atmospheres using AVHRR Daytime Imagery. *Geophysical Research Letters*, 24, 1791-1794.

Hutchison, K. D., B. J. Etherton, and P. C. Topping (1997). Validation of automated cloud top phase algorithms: distinguishing between cirrus clouds and snow in a-priori analyses of AVHRR imagery. *Optical Engineering*., 36, 1727-1737.

Hutchison, K. D., B. J. Etherton, P. C. Topping, and A. H. L. Huang (1997). Cloud Top Phase Determination from the Fusion of Signatures in Daytime AVHRR Imagery and HIRS Data. *International Journal of Remote Sensing*, 18, 3245-3262.

Hutchison, K. D., K. Hardy, and B. C. Gao (1995). Improved detection of optically-thin cirrus clouds in nighttime multispectral meteorological satellite imagery using total integrated water vapor information. *Journal of Applied Meteorology,* 34, 1161-1168.

King, M. D., W. P. Menzel, P. S. Grant, J. S. Myers, G. T. Arnold, S. E. Platnick, L. E. Gumley, S. C. Tsay, C. C. Moeller, M. Fitzgerald, K. S. Brown, and F. G. Osterwisch (1996). Airborne Scanning Spectrometer for Remote Sensing of Cloud, Aerosol, Water Vapor, and Surface Properties. *J. Atmos. Oceanic Technol.*, 13, 777-794.

Kriebel, K. T., and R. W. Saunders (1988). An Improved Method for Detecting Clear Sky and Cloudy Radiances from AVHRR Data. *Int. J. Remote Sens*., 9, 123-150.

Lou, G., P. A. Davis, L. L. Stowe, and E. P. Mcclain (1995). A pixel-scale algorithm of cloud type, layer, and amount for AVHRR data. Part I: Nighttime, *Journal of Atmospheric and Oceanic Technology*, 12, 1014-1036.

McClain, E. P. (1993). Evaluation of CLAVR Phase-I Algorithm Performance: Final Report, U.S. Department of Commerce/NOAA/NESDIS. Report 40-AANE-201-424.

Rossow, W. B. (1989). Measuring Cloud Properties from Space: A Review. *J. Clim*., 2, 201.

Saunders, R. W. and K. T. Kriebel, (1988). An improved method for detecting clear sky and cloudy radiances from AVHRR data, *International Journal of Remote Sensing*, 9, 123-150.

Stamnes, K., W. Li, X. Xiong, and B. Chen (1998). Remote Sensing of Cloud and Surface Properties in Polar Regions from GLI Measurements on Board ADEOS-II. The 3rd GLI Workshop, Tokyo.

Stowe, L. L., P. Davis, and E. P. McClain (1995). Evaluating CLAVR (Clouds from AVHRR) Phase I Cloud Cover Experimental Product. *Adv. in Space Res*., 16, 21-24.

Stowe, L. L., P. Davis, and E. P. McClain (1998). Scientific Basis and Initial Evaluation of the CLAVR-I Global Clear/Cloud Classification Algorithm for the Advanced Very High Resolution Radiometer, *J. Atmos. and Oceanic Technology*, submitted May 1st.

Strabala, K. I., S. A. Ackerman, and W. P. Menzel (1994). Cloud Properties Inferred from 12 micron Data, *J. Appl. Meteor*., 33, 212-229.

Valvocin, F. R. (1978). Spectral radiance of snow and clouds in the near infrared spectral region. *Tech Report No. 78-0289*, Air Force Geophysics Laboratory, Hanscom Air Force Base, MA.